Neurovascular coupling is preserved in chronic stroke recovery after targeted photothrombosis

Smrithi Sunil [a,*], John Jiang [a], Shashwat Shah [a], Sreekanth Kura [a], Kivilcim Kilic [a], Sefik Evren Erdener [b], Cenk Ayata [c], Anna Devor [a,d], David A. Boas [a,*]

[a] *Department of Biomedical Engineering, Boston University, Boston, MA 02215, USA*
[b] *Institute of Neurological Sciences and Psychiatry, Hacettepe University, Ankara, Turkey*
[c] *Departments of Neurology and Radiology, Massachusetts General Hospital, Boston, MA 02114, USA*
[d] *Athinoula A. Martinos Center for Biomedical Imaging, Massachusetts General Hospital, Boston, MA 02114, USA*

ARTICLE INFO

ABSTRACT

Functional neuroimaging, which measures hemodynamic responses to brain activity, has great potential for monitoring recovery in stroke patients and guiding rehabilitation during recovery. However, hemodynamic responses after stroke are almost always altered relative to responses in healthy subjects and it is still unclear if these alterations reflect the underlying brain physiology or if the alterations are purely due to vascular injury. In other words, we do not know the effect of stroke on neurovascular coupling and are therefore limited in our ability to use functional neuroimaging to accurately interpret stroke pathophysiology. To address this challenge, we simultaneously captured neural activity, through fluorescence calcium imaging, and hemodynamics, through intrinsic optical signal imaging, during longitudinal stroke recovery. Our data suggest that neurovascular coupling was preserved in the chronic phase of recovery (2 weeks and 4 weeks post-stoke) and resembled pre-stroke neurovascular coupling. This indicates that functional neuroimaging faithfully represents the underlying neural activity in chronic stroke. Further, neurovascular coupling in the sub-acute phase of stroke recovery was predictive of long-term behavioral outcomes. Stroke also resulted in increases in global brain oscillations, which showed distinct patterns between neural activity and hemodynamics. Increased neural excitability in the contralesional hemisphere was associated with increased contralesional intrahemispheric connectivity. Additionally, sub-acute increases in hemodynamic oscillations were associated with improved sensorimotor outcomes. Collectively, these results support the use of hemodynamic measures of brain activity post-stroke for predicting functional and behavioral outcomes.

1. Introduction

An ischemic stroke occurs due to interruption of cerebral blood flow caused by thrombosis or embolism of a blood vessel, which leads to a reduction or complete loss of blood supply to downstream brain areas. Loss of blood supply causes a starved oxygen environment and leads to cellular damage within minutes and ultimately to sensorimotor and cognitive impairments (Moskowitz et al., 2010; Lo et al., 2005). A majority of stroke patients survive the incident, however, most survivors are compromised in work capacity, the extent of which varies across patients from mild to severe impairments (Sharma and Cohen, 2012). Some spontaneous recovery is typically seen in most patients in the months following injury and most post-stroke recovery currently relies heavily on rehabilitative treatments (Cramer, 2008; Cassidy and Cramer, 2017; Jones, 2017).

Functional neuroimaging methods, such as functional magnetic resonance imaging (fMRI) and functional near-infrared spectroscopy (fNIRS), which measure the hemodynamic response to brain activity, have the potential for being valuable tools for monitoring and managing the recovery and treatment of stroke patients both in the acute and chronic phases of stroke recovery (Moseley, 2010; Veldsman et al., 2015; Lake et al., 2016). However, the hemodynamic responses post-stroke are almost always altered relative to those seen in healthy individuals. Blood-oxygen-level-dependent fMRI (BOLD-fMRI) studies have revealed that task-related cortical responses following stroke undergo pronounced alterations in amplitude and spatial extent of the

BOLD signal in both the ipsilesional and the contralesional hemispheres (Lake et al., 2016; Johansen-Berg et al., 2002; Pineiro et al., 2002). Additionally, studies assessing resting-state functional connectivity obtained with MRI (rs-fMRI) have shown that inter-hemispheric connections are altered in the early acute phase of stroke in humans (Carter et al., 2009; Corbetta, 2012). Longitudinal rs-fMRI studies have shown to be valuable to track stroke recovery progression as well as a biomarker of improved recovery (Blaschke et al., 2021; Park et al., 2011). Whether these hemodynamic response alterations reflect the underlying differences in neural function or simply a result of injury to the vasculature is still under active investigation. In other words, we do not know the effect of stroke on neurovascular coupling and thus are limited in our ability to use these valuable neuroimaging tools to study functional recovery in stroke survivors.

Neurovascular coupling (NVC) has been studied extensively in healthy subjects and there is a large body of evidence suggesting that neural activity is closely related to cerebral blood flow (CBF) and oxygen metabolism (Kleinfeld, 2011; Buxton et al., 2014). This tight coupling between neural activity and hemodynamics forms the basis of modern neuroimaging techniques that use the cerebrovascular changes caused by neural activation to map changes in function in the behaving human brain (Logothetis et al., 2001). While NVC is maintained in the healthy brain, brain pathologies such as traumatic brain injury, Alzheimer's disease, and stroke may lead to disruptions in the interactions between neural activity and CBF, leading to neurovascular uncoupling, thereby confounding interpretations of neuroimaging results (Kunz and Iadecola, 2009; Girouard and Iadecola, 2012). Additionally, the effect of stroke on NVC has received limited attention and sometimes led to conflicting results (Lake et al., 2016; Weber, 2008; Shih, 2014). Thus, there is a need for preclinical stroke models to evaluate the functional aspects of neurovascular recovery and to use these findings to improve the interpretations of human neuroimaging studies.

Preclinical animal models of stroke have been used extensively over the last few decades to understand the mechanisms involved in stroke recovery from molecular and cellular changes to large scale functional network reorganizations (Carmichael, 2005; modeling cerebral ischemia, 2010; Sommer, 2017). On a mesoscopic level, studies performing in vivo calcium fluorescence imaging of neural activity and intrinsic optical signal imaging (IOSI) of hemodynamic activity have shown activation reorganization and functional remapping of the stroke affected brain regions in the peri-infarct zone longitudinally, bearing on physiological processes underlying the evolution of stroke in humans (Winship and Murphy, 2008; Brown et al., 2009; Harrison et al., 2013; Clarkson, 2013). Additionally, calcium imaging, IOSI, and rs-fMRI have all been implemented in animal models to study changes in resting state functional brain connectivity to assess global changes as well as responses to functional activation (van Meer, 2010; Lim et al., 2014; Bauer et al., 2014; Cramer et al., 2019). To improve interpretations of human functional neuroimaging studies and to understand the underlying physiology that gives rise to the observed hemodynamic signals we need to obtain simultaneous measures of neural and hemodynamic parameters post-stroke. Moreover, these measures need to be obtained on a mesoscopic scale to understand both the local and global changes that result due to stroke, as well as cover the entire longitudinal recovery phase to capture both acute and chronic time points.

Prior work on functional recovery following ischemic stroke has focused either primarily on neural or hemodynamic activity changes or just the acute or chronic phase of stroke recovery (Park et al., 2011; Winship and Murphy, 2008; Lim et al., 2014; Bauer et al., 2014; Schrandt et al., 2015). Only limited work has been done on integrating neural and hemodynamic measures to study neurovascular recovery after stroke (He, 2020). He et al. 2020 combined flexible intracortical electrode arrays and laser speckle contrast imaging (LSCI) to simultaneously measure local field potentials, spiking activity, and cerebral blood flow during chronic stroke recovery in the somatosensory cortex. They observed significant neurovascular disassociation immediately

after stroke and into the sub-acute phase. Further, the severity of neurovascular disassociations in the chronic phase was associated with the degree of initial injury (He, 2020). These results reveal the limitations of functional neuroimaging as a reliable measure of underlying neural activity in the acute and sub-acute phases of stroke recovery. However, behavioral assessments were not performed, and it remains to be seen how neurovascular coupling is associated with behavioral recovery.

In this exploratory study, we utilized a wide-field multimodal imaging technique, that can simultaneously monitor neural activity and hemodynamic changes longitudinally during stroke recovery, to study the evolution of neurovascular coupling (NVC) across the surface of the brain. We report on several neuroimaging measures that can be used as biomarkers for NVC and understand their progression along with behavioral recovery. We have previously established an optimized photothrombotic stroke model that more closely mimicked the physiology of a human stroke by inducing a stroke in an awake animal, occluding a single arteriole, and eliciting a distinct core and peri-infarct region (Sunil et al., 2020). Traditional photothrombosis suffers from the lack of a graded penumbra making it difficult to follow recovery mechanisms. But by modifying photothrombosis to only target a surface arteriole and thereby maintaining the integrity of the underlying and surrounding tissue, as validated in our previous work, we produce a graded stroke core and peri-infarct region that can be monitored during chronic recovery. Here, we show that our optimized stroke model together with wide-field neural calcium and hemodynamic imaging can be used to monitor neurovascular coupling longitudinally. Our exploratory results suggest that neurovascular coupling, as established using pre-stroke neural activity and hemodynamics, is maintained in the chronic phase of stroke recovery, implying that functional neuroimaging measurements faithfully represent the underlying neural activity in the chronic phase. Additionally, our data revealed increases in global brain oscillations in the acute phase of recovery and showed distinct patterns of oscillations for neural and hemodynamic activity. The extent of ischemia, neurovascular uncoupling, and hemodynamic oscillations in the sub-acute phase were predictive of behavioral recovery in the chronic phase. To the best of our knowledge, this is the first comprehensive paper to study and model neurovascular coupling across both hemispheres of the brain during chronic stroke recovery along with behavioral assessments.

2. Results

To study longitudinal neurovascular coupling during stroke recovery, we implemented a multimodal photothrombosis and imaging system that can perform targeted photothrombosis, as well as wide-field fluorescence imaging, intrinsic optical signal imaging, and spatial frequency domain imaging. All experiments were performed in adult Thy1-GCaMP6f mice implanted with bilateral cranial windows. After a two-week recovery and habituation period, baseline imaging was performed to obtain pre-stroke measures of tissue optical properties as well as resting state and sensory evoked neural activity and hemodynamics to assess healthy neurovascular coupling. Photothrombosis to the pial artery supplying blood to the right forelimb was performed on Day0. A unique feature of targeted photothrombosis is the natural variability in stroke sizes, as we would expect in human strokes (Supplementary figure 1). Follow-up imaging was performed at Day2, Week1, Week2, and Week4 to span acute (Day2), sub-acute (Week1), and chronic (Week2 and Week4) phases of stroke recovery. In all figures, the right hemisphere, which received the stroke, is the ipsilesional hemisphere and the left hemisphere is the contralesional hemisphere. Fig. 1a shows a simplified schematic of the imaging system and the experimental timeline. At each time point, first, spatial frequency domain imaging (SFDI) was performed to obtain tissue absorption and scattering coefficients. Tissue scattering at Week1 was used to determine the stroke core area, peri-infarct region, and healthy tissue in subsequent analysis. Fig. 1b shows the scattering coefficients (top) at four time points and the
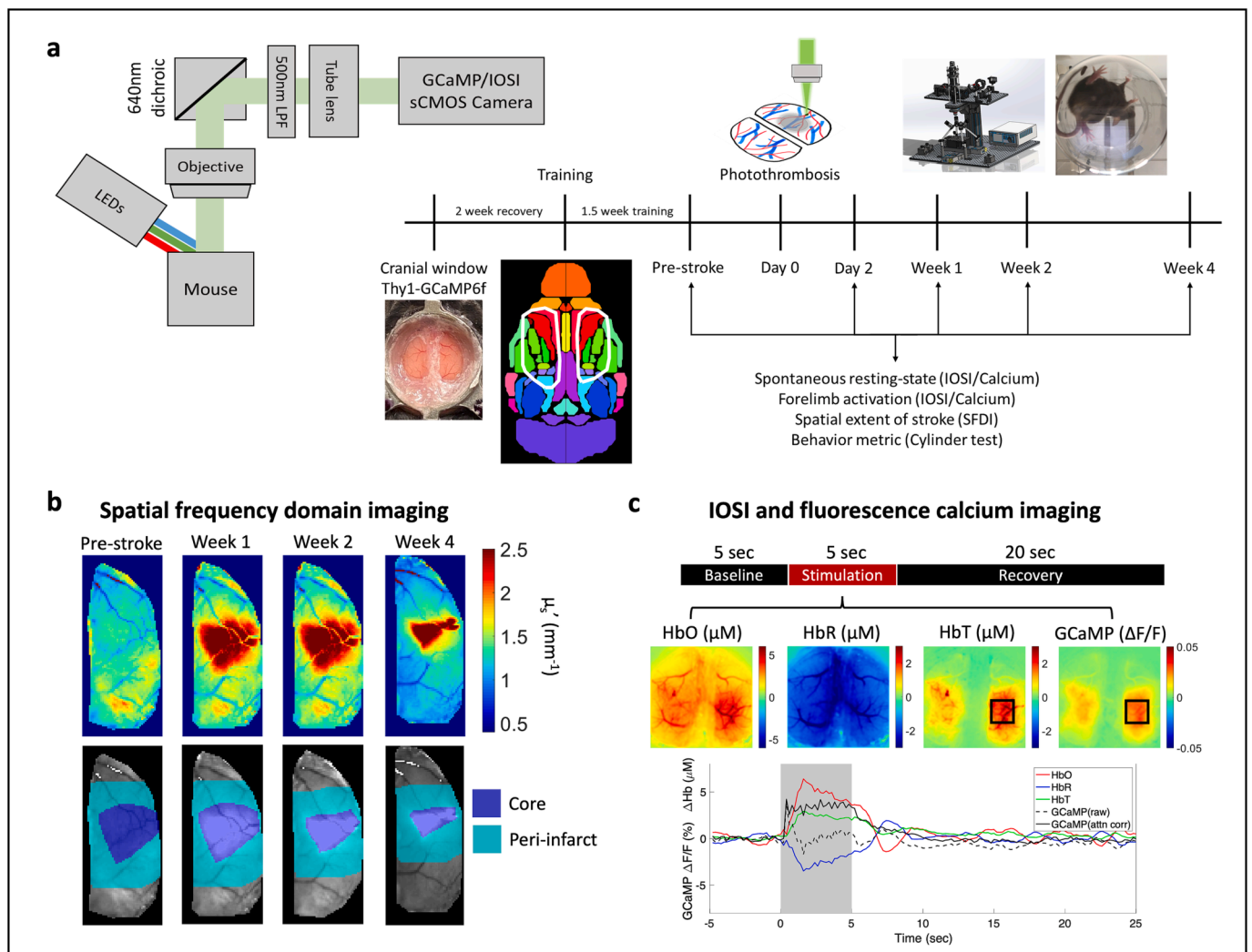
Fig. 1. Multimodal imaging of neurovascular coupling for monitoring longitudinal stroke recovery. (a) Simplified imaging schematic and experimental timeline. Note: Imaging schematic only shows green light reflected for convenience, however, all reflected light between 500mn and 640 nm is captured by the camera. (b) SFDI. Top: Tissue scattering coefficients at each time point. Bottom: Stroke core and *peri*-infarct regions for the above images. (c) Sensory stimulation with IOSI. Top: Block design of each trial in a stimulation session, middle: trial averaged spatial maps of HbO, HbR, HbT, and corrected GCaMP, during 5 *sec* of air-puff stimulation to the left forelimb, bottom: trial averaged time course of each measurement, note that raw uncorrected GCaMP drops immediately following the rise of the hemodynamic response and corrected GCaMP shows elevated responses through the full stimulation period. (For interpretation of the references to colour in this figure legend, the reader is referred to the web version of this article.)

corresponding core and peri-infarct outlines (bottom) for an example mouse. Day2 was not used for infarct quantification as the tissue is still very dynamic in the acute phase. Week1 was used as the first stable time point for tissue properties assessment with SFDI. Following SFDI, simultaneous IOSI and fluorescence imaging were performed for 10 min during resting state and then for 10 min with sensory stimulation. Sensory stimulation using air-puff to the forelimb was performed in a block design paradigm (Fig. 1c) and included 5 *sec* of baseline, followed by 5 *sec* of 3 Hz stimulation to the contralateral or ipsilateral forelimb, followed by 20 *sec* of rest before the next trial. Each trial was repeated 20 times in one session. Fig. 1c shows an example of the spatial maps and time-course of stimulus induced response in a healthy mouse. The raw GCaMP fluorescence signal was corrected for hemodynamic crosstalk using Beer-Lambert calculations with the simultaneously obtained changes in oxy- and deoxy-hemoglobin. We employed a modified attenuation estimation method (detailed in the Methods section) to obtain absorption, scattering, and pathlength factors of the tissue, prior to hemodynamic correction analysis (Ma, 2016; Ma, 2016) (Fig. 1c, Supplementary figure 2). Note that hemodynamic correction is typically applied to correct for the crosstalk within parenchymal tissue where

tissue is more homogeneous and pathlength estimation is more accurate. The Beer-Lambert calculations used the same pathlength factor for every pixel outside the stroke core area. This correction method has been shown to be inadequate for large pial vessels due to variations in optical properties (Valley, 2020). Therefore, appearance of large vessels on the surface even after hemodynamic correction is due to the inaccuracy of the Beer-Lambert calculations for large blood vessels.

2.1. Wide-field fluorescence and intrinsic optical signal imaging can simultaneously follow changes in neural calcium and hemodynamic activity after stroke

Neurovascular coupling has been studied extensively in healthy subjects in both humans and animal models. In rodents, wide-field fluorescence calcium and intrinsic optical hemodynamic signals have been imaged simultaneously to investigate the baseline relationships between neural activity and blood flow (Ma, 2016; Wright et al., 2017). Imaging calcium dynamics using GCaMP has been used extensively over the last decade as a correlate and reliable metric of neural activity (Tian, 2009; Dana et al., 2014). Here, we first implemented these techniques to

show that wide-field optical imaging can be used to investigate the differential effects of stroke on neural calcium dynamics and cerebral blood volume assessed with changes in the concentration of oxy and deoxy hemoglobin (HbO and HbR respectively). We first assessed alterations to evoked responses during sensory stimulation after stroke.

Unilateral photothrombotic stroke to the forelimb somatosensory cortex of the right hemisphere led to a significant suppression of the evoked calcium and hemodynamic responses to air-puff stimulation of the contralateral (affected) forelimb within the affected hemisphere, while the responses in the unaffected hemisphere were preserved (Fig. 2a,b). The largest suppression of the response occurred 2 days post-stroke with a slow return of the response by 4 weeks, albeit still suppressed compared to pre-stroke. At day 2 after stroke, GCaMP showed a 70 % reduction in the response. At the same time, total hemoglobin (HbT) showed an almost complete reduction in response and HbO showed a 45 % reduction in response, compared to pre-stroke baseline (Supplementary Figure 4a). By 4 weeks after stroke the responses within the affected hemisphere had returned to 50 % of the pre-stroke value for

GCaMP and hemodynamics. Evoked responses to forelimb air-puff stimulation of the unaffected forelimb did not exhibit significant alterations in the contralateral (unaffected) hemisphere, however, the affected hemisphere showed suppressed responses (Fig. 2c,d). Once suppressed, the affected hemisphere did not recover either GCaMP or hemodynamic responses to ipsilateral (unaffected) forelimb stimulation even at 4 weeks (Supplementary figure 4b). Spatiotemporal maps of responses during baseline, stimulation, and recovery at each time point are shown in Supplementary Fig. 5 for the same mouse shown in Fig. 2a, c. Knowing the co-evolution of neural and hemodynamic responses can aid in better interpretations of the alterations observed in the hemodynamic fMRI signals after stroke. The results here show that wide-field fluorescence and intrinsic optical signal imaging following photothrombotic stroke are sensitive measures that allow the longitudinal monitoring of these neural and hemodynamic signals.
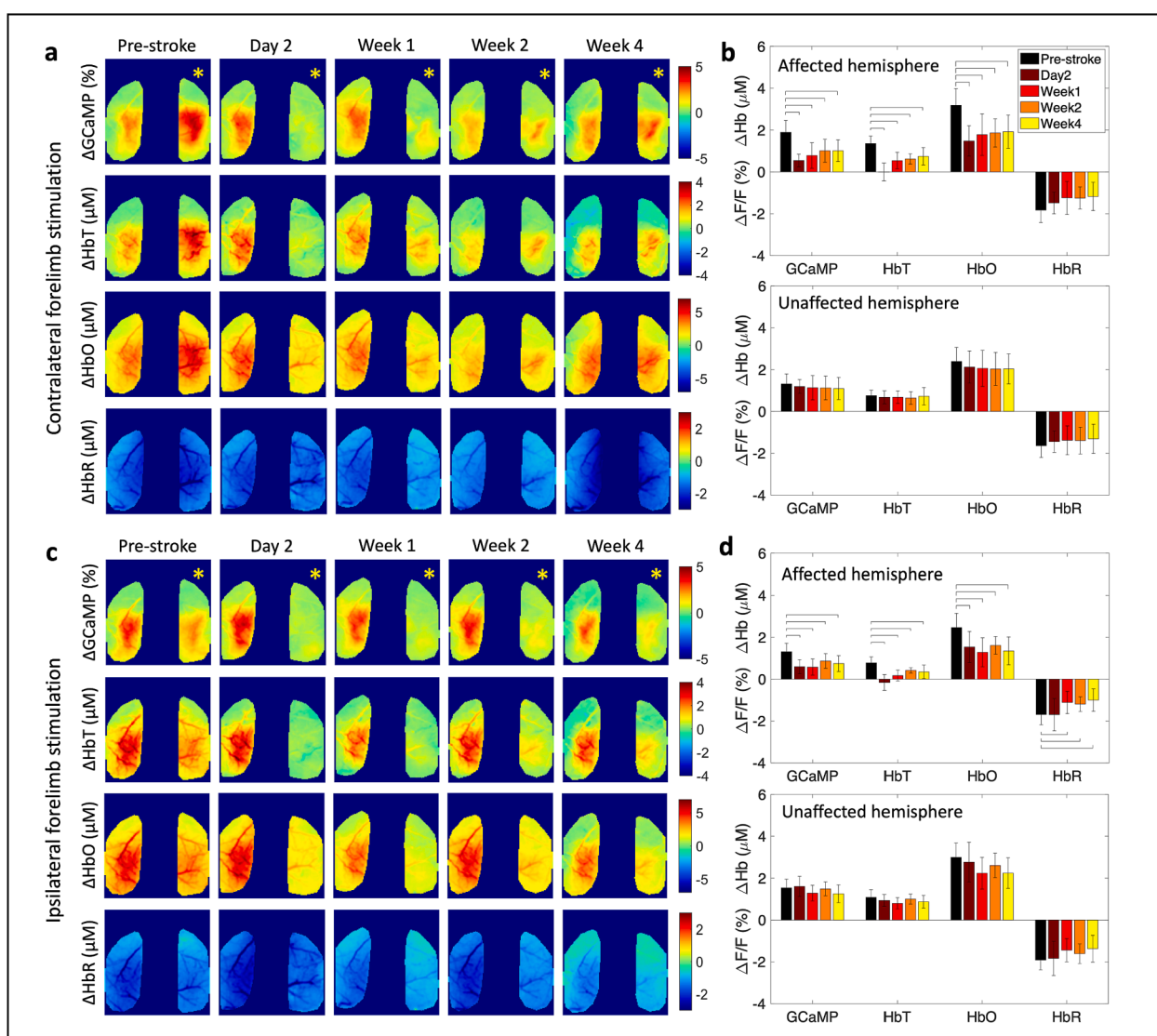

Fig. 2. Simultaneous calcium and hemodynamic imaging post-stroke. (a) Trial-averaged spatial maps of calcium and hemodynamics showing magnitude of the response during 5-*sec* stimulation of the contralateral (affected) forelimb at each time point before and after stroke in one example mouse. (b) Response magnitudes during affected forelimb stimulation for all mice (n = 12) in the affected (top) and unaffected (bottom) hemispheres, histograms are mean ± std. (c) Same as in (a) during stimulation of the ipsilateral (unaffected) forelimb. (d) Same as in (b) during stimulation of the ipsilateral (unaffected) forelimb. A two-sample *t*-test was run for all statistical tests. Bars in (b) and (d) indicate significance of p < 0.05. Yellow asterisk indicates stroke hemisphere. (For interpretation of the references to colour in this figure legend, the reader is referred to the web version of this article.)

2.2. Trial-by-trial correlations of sensory activation reveal variability in neurovascular recovery patterns across mice

To evaluate NVC, we examined whether aspects of the observed hemodynamic responses were correlated with the underlying calcium activity during sensory stimulation of the impaired forelimb. Fig. 3a shows the trial-averaged mean and standard deviation of the time course of calcium, measured as a percent change in fluorescence (top row), and change in HbO and HbR, measured in μM (bottom row), averaged from all pixels within the affected hemisphere at pre-stroke, 1 week, and 4 weeks post-stroke. Spatial response maps, obtained during the 5-*sec* stimulation period, were then thresholded at each time point to 75 % of the peak response and all pixels that lie above that threshold were used for correlation analysis (Fig. 3b). A threshold of 75 % provided the largest well-connected boundary for the forelimb region. Thresholds lower than 70 % produced patches of activation in regions farther away from the expected forelimb and thresholds above 80 % underestimated the forelimb regions. We first examined the similarity in the response areas between the evoked calcium response and hemodynamic measures. Similarity was calculated using the Dice coefficient, which provides a measure of the percent overlap, or union, of two images (Fig. 3c).

HbT and HbO showed high overlap (60 %) with GCaMP before the stroke, indicating that GCaMP and hemodynamic responses were spatially localized, while HbR had a weaker spatial overlap with GCaMP (20 %). These values of activity localization are expected as shown in prior work where hemodynamic responses have larger spatial extent compared to neural activation (Erinjeri and Woolsey, 2002; Lake, 2020) and HbT is more localized compared to HbR (Culver et al., 2005). However, it should be noted that the dice coefficient with our imaging modality provides a two-dimensional spatial representation and does not account for any changes in the volume of activation. Within the ipsilesional hemisphere, HbT and HbO showed a significant reduction in the spatial overlap with GCaMP across all time points after stroke, with a larger reduction in the acute time points of day 2 and week 1 compared to chronic time points. In contrast, the overlap between HbR and GCaMP was not significantly altered. GCaMP and hemodynamic response maps in the contralesional hemisphere were not significantly altered after stroke (Supplementary figure 7a).

Next, we calculated the average magnitude of the response during 5 s of air-puff stimulation within all pixels above 75 % of peak activation. We then correlated the magnitude of the GCaMP response to the magnitude of the HbO and HbR responses for each stimulus trial. Fig. 3d
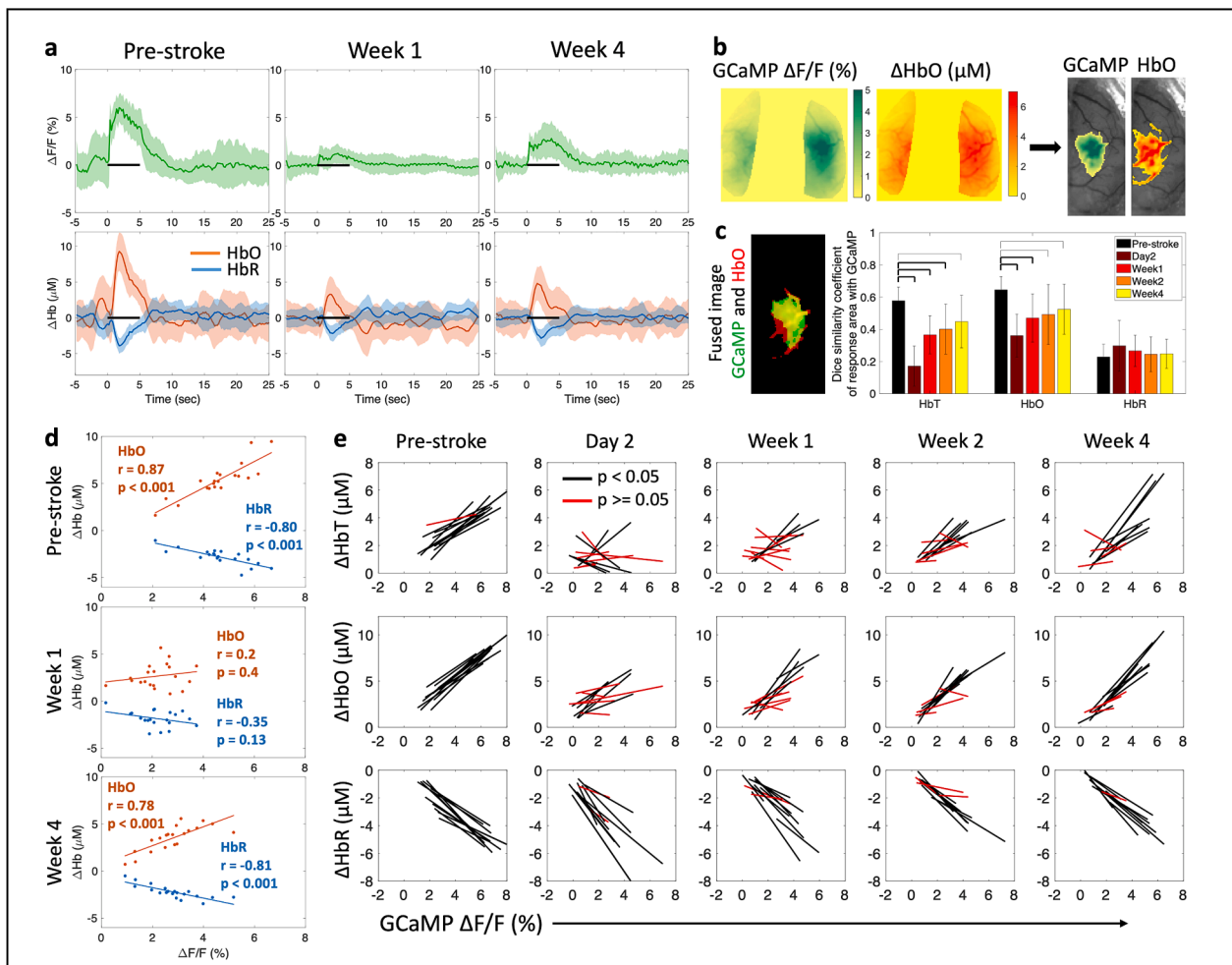

Fig. 3. Correlation between evoked calcium and hemodynamic responses. (a) Trial-averaged time-course showing mean (±std) of GCaMP (top) and HbO and HbR (bottom) for all pixels within the affected hemisphere at the pre-stroke baseline, 1 week, and 4 weeks post-stroke. Note the drop in response to stimulation (black bar) at week 1. (b) Threshold algorithm applied to GCaMP and Hb responses. (c) Overlap between the response area of GCaMP and HbO, left: single trial fused image for reference, GCaMP is green, HbO is red, and overlap region is yellow, right: Dice similarity coefficients across all mice (n = 12) and time points. Thick bars: p < 0.01, thin bars: p < 0.05. (d) Correlation of response magnitudes between GCaMP and HbO and HbR for one mouse at pre-stroke, week 1, and week 4. Inset numbers represent correlation value and significance of fit. (e) Correlation of calcium and hemodynamics across all mice (n = 12) over all time points; each line represents one mouse. A two-sample *t*-test was run for all statistical tests. Black lines represent significant correlation and red lines represent no significance. (For interpretation of the references to colour in this figure legend, the reader is referred to the web version of this article.)

shows an example pre- and post-stroke dataset from one mouse; each dot in the scatter plot represents data from one trial within a block of 20 trials. There was high correlation between the evoked GCaMP responses and HbO, as well as GCaMP and HbR, prior to stroke, demonstrating that we can use trial-by-trial information to establish pre-stroke activity correlations as well as showing healthy coupling between neural activity and hemodynamics. The correlation was lost 1 week after stroke and recovered by 4 weeks. This evolution of correlation was seen across the cohort of animals (Fig. 3e). Both HbT and HbO showed significant loss in correlation with GCaMP in the acute phase, implying that calcium responses in the acute phase were not necessarily represented in the observed hemodynamic response. However, this loss in correlation in the acute phase could also be due to the small amplitudes of the signal, which can result in larger noise and thus low correlation. Additionally, those mice that had a residual loss of correlation at week 4 compared to those that fully recovered, also had a worse correlation between GCaMP and HbT/HbO responses in the acute phase (Supplementary figure 6). The correlation between calcium and hemodynamic responses in the contralesional hemisphere was preserved throughout the recovery period (Supplementary figure 7b).

2.3. Healthy hemodynamic response function can be used to predict neurovascular coupling in chronic stroke recovery

The next question we asked was whether the shape of stimulus-induced neurovascular response was preserved across the acute and chronic phases of stroke recovery. To that end, we estimated a hemodynamic response function (HRF) (or impulse response function (IRF)), which is the kernel that, when convolved with the GCaMP signal, provides an estimate of the hemodynamic activity. Linear least-squares deconvolution was used to estimate the HRF from the data as established previously (Ma, 2016; Montgomery, 2020). First, we validated the method using the baseline (pre-stroke) data. We calculated the HRF using the entire time-course for all pixels that responded to forelimb air-puff stimulation (>75 % of peak response) in HbT maps (Fig. 4a, top). We observed the expected and characteristic shape of the HRF, a post-stimulus overshoot, peaking at approximately 1 sec following stimulation, followed by an undershoot, as reported previously (Ma, 2016; Lake, 2020). Next, we applied the same procedure to data collected 2 days following stroke using the same brain region that originally responded to forelimb stimulation. This analysis resulted in a distinctly altered HRF, suggesting a disruption to neurovascular coupling (Fig. 4a, bottom). Fig. 4b shows the time-course of four individual stimulation trials; the measured GCaMP signal is overlaid with the measured HbT and estimated HbT, where the estimated HbT was obtained by convolving the GCaMP signal with the time-point specific HRF kernel. Pre-stroke, the measured and estimated HbT showed good overlap (Fig. 4b, top), while at day 2 after stroke the overlap was poor (Fig. 4b, bottom). Additionally, at day 2 after stroke, there was no response to stimulation, and we observed large oscillations in the measured hemodynamic signal. A Pearson's correlation coefficient was calculated between the measured and estimated HbT signal at each pixel for both hemispheres of the brain to assess the goodness-of-fit (Fig. 4c), and we observed high correlation across the somatosensory cortex in both hemispheres before the stroke (Fig. 4c, top). This suggests that hemodynamic activity was coupled to the underlying calcium activity prior to stroke. Regions closer to motor cortex showed lower correlation compared to regions within sensory cortex. Higher correlation in the sensory cortex could be due to the presence of air-puff stimulus, which could be driving both calcium and hemodynamic responses and strengthening our observation of neurovascular coupling. This hypothesis can be validated by comparing the HRF and correlation obtained during resting-state and sensory stimulation sessions. Prior work has shown that neural activity is more weakly correlated to hemodynamics during resting state and was validated by our data (Supplementary figure 8) (Winder et al., 2017). Our resting-state data still show a

relatively high correlation, which could be due to natural behavior of the mouse, such as whisking and grooming, driving cortical activity. At day 2 after stroke there was a loss in correlation between the measured and predicted HbT as indicated by drop in the Pearson's correlation coefficient (Fig. 4c, bottom).

The same convolution model was applied to calcium and hemodynamic data to estimate the HRF post-stroke across all animals and time points. The post-stroke HRF was calculated for the stroke core, the peri-infarct region, which included all the pixels within 0.5 mm from the stroke core boundary, and the contralesional forelimb region. The HRF was also calculated for HbO and HbR in addition to HbT. Fig. 4d shows an example mouse where the stroke core, peri-infarct, and contralesional forelimb are highlighted in black. We then followed the evolution of the HRF for each hemodynamic measure after stroke. Fig. 4e shows the mean and standard deviation of the HRF for one example mouse. We observed a significant deviation in the HRF within the stroke core and peri-infarct region in the acute phase of recovery. Following the acute phase, the chronic phase showed a recovery in the HRF. The contralesional HRF remained largely unaffected by the stroke. Similar trends were observed across all animals (Fig. 4f), where acute stroke resulted in deviation of the HRF in the core and peri-infarct, while the contralesional hemisphere was unaffected. In the chronic phase the HRF showed better recovery of the shape, with respect to pre-stroke HRF, in the peri-infarct region. The HRF within the stroke core continued to show deviation in some animals.

Here, we describe deviation of the HRF in terms of the qualitative similarity of shape to the pre-stroke HRF. However, even if the shape of the HRF is different, it could still be used to accurately predict hemodynamics. Therefore, we next tested the ability of the HRF at each time point to predict hemodynamics. Supplementary figure 9a shows a pixel-by-pixel map of the Pearson's correlation coefficient for one example mouse for all three hemodynamic measures before and after stroke. We observed a clear drop in correlation coefficient within the affected hemisphere, specifically in day 2. Over time, through the recovery period, we observed a return of correlation between the measured and predicted hemodynamics in the peri-infarct region. The correlation coefficient was quantified across all mice in the stroke core, peri-infarct, and contralesional forelimb region (Supplementary figure 9b).

From the shape of the HRF we can clearly see that the neurovascular coupling model is not behaving as expected during day 2 and week 1. Most notably, we see that the HRF is not flat prior to stimulus onset at time = 0 as we would expect. We have provided more flexibility in our model by allowing it to use GCaMP events that have not happened yet to find the best fit. In the pre-stroke case this negative time region is a flat line at zero indicating that future GCaMP events have no influence on the current hemodynamics, as expected. While it is physiologically not possible for future GCaMP events to influence current hemodynamics, this deviation in the HRF indicates that there are possibly additional dynamics that are not captured by the original model and the model is trying to find the best fit with the given data. We can overcome this limitation and test deviations in neurovascular coupling by testing how well we are able to predict the post-stroke hemodynamics with the pre-stroke HRF, since we know that the pre-stroke HRF is behaving as expected. To test alterations to neurovascular coupling, we calculated the mean HRF for each mouse from pre-stroke "healthy" data and convolved the pre-stroke HRF with the post-stroke GCaMP time-course and obtained the correlation with the predicted and measured hemodynamics (Fig. 4g). Like the time-point specific HRF, there was a significant drop in correlation within the stroke and per-infarct regions in the acute phase and a recovery within the peri-infarct region in the chronic phase when using the pre-stroke "healthy" HRF (Fig. 4h). Unlike the time-point specific HRF correlations (Supplementary figure 9), the healthy HRF correlations with post-stroke data showed virtually no correlation between the measured and predicted HbT and only a small correlation in HbO at day 2. However, the healthy pre-stroke HRF was able to predict hemodynamic activity with high accuracy in the chronic phase of stroke
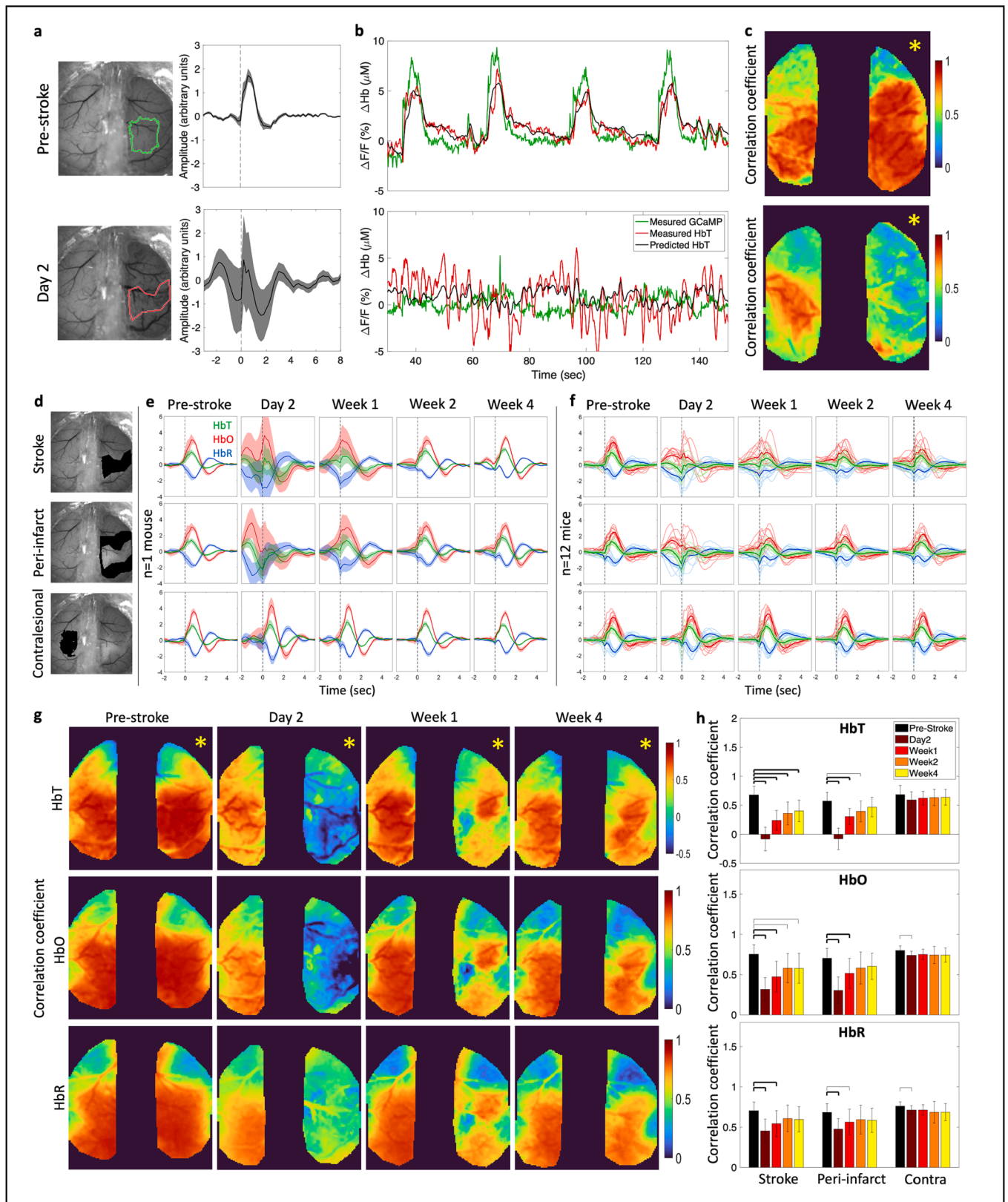
(caption on next page)

Fig. 4. Neurovascular coupling with linear least-squares deconvolution. (a) Hemodynamic response function (HRF) before (top) and 2 days after stroke (bottom) in the forelimb and stroke regions outlined in green and red respectively. (b) Time course of 4 stimulation trials showing measured GCaMP signal overlaid with measured HbT and predicted HbT, obtained by convolving the GCaMP signal with the HRF kernel, at pre-stroke and day 2 for the regions outlined in (a). (c) Pearson's correlation coefficient for measured HbT and predicted HbT for pre-stroke (top) and 2 days after stroke (bottom). (d) Regions used to extract HRF in (e) and (f). (e) HRF obtained by deconvolution model for HbT, HbO, and HbR, for one example mouse at each time point before and after stroke. Note the deviation in HRF compared to pre-stroke in the acute phase within the stroke and *peri*-infarct, and a return to pre-stroke HRF at week 4. (f) Same as in (e) for all mice (n = 12). Each line represents the HRF for one mouse. (g) Pixel-by-pixel Pearson's correlation coefficient between measured and predicted HbT (top), HbO (middle), and HbR (bottom). Predicted HbX is obtained by convolving the GCaMP signal at each time point with a mean HRF obtained from pre-stroke data. (h) Pearson's correlation coefficient quantified across all mice within the stroke core, *peri*-infarct, and contralesional forelimb region. A two-sample *t*-test was run for all statistical tests. Thick bars: p < 0.01, thin bars: p < 0.05. Note the sustained reduction of correlation coefficient within the stroke core but recovery within the *peri*-infarct for HbT and HbO. Yellow asterisk indicates stroke hemisphere. (For interpretation of the references to colour in this figure legend, the reader is referred to the web version of this article.)

recovery. A reestablishment of the correlation in the peri-infarct region at week 4 using the pre-stroke HRF suggests that the recovery is associated with a return to "healthy" neurovascular coupling and not a new coupling relationship between neural and hemodynamic activity. This in turn indicates that functional neuroimaging methods, when used in the chronic recovery period, faithfully represent the underlying neural activity.

2.4. Acute stroke leads to increases in global brain oscillations

Stroke is known to have a profound effect not only on the local network but also on the contralesional and subcortical networks of the brain. In our neurovascular coupling analysis, we observed an increase in oscillatory dynamics in the hemodynamic signal. Through our widefield imaging approach we can assess the effect of stroke on both hemispheres of the brain during resting-state. To assess brain-wide variations in the signals we first investigated the overall change to signal patterns. Fig. 5a shows the resting-state time-courses of GCaMP and HbO signals at pre-stroke and 2 days post-stroke within the ipsilesional peri-infarct (Fig. 5a, top) and the contralesional forelimb regions (Fig. 5a, bottom) that was filtered at 0.009–0.4 Hz, which covers the low and high frequency hemodynamic signal ranges used in prior work (Wright et al., 2017). A feature of note here is the increase in amplitude of the HbO signal at day 2 in the ipsilesional hemisphere (light red line in Fig. 5a top) compared to pre-stroke, but an increase in amplitude of both the HbO and GCaMP signal at day 2 within the contralesional hemisphere. We validated this increase in amplitude by calculating the variance in the overall signal (Fig. 5b). GCaMP showed only minor alterations in variance while HbO showed a large increase in the variance of its signal at day 2, which was resolved by week 4. To address whether this increase in the amplitude of the signal was across all frequencies or specific to a particular frequency, we calculated the power spectrum of the GCaMP and hemodynamic signal within the affected and unaffected hemisphere (Fig. 5c). There was an overall increase in amplitude across all frequencies at 2 days after stroke in the HbO signal of the ipsilesional hemisphere. Moreover, there was a significant increase in amplitude of the hemodynamic signal at 2 days and 1 week after stroke at specifically around 0.25 Hz within the ipsilesional hemisphere. The contralesional hemisphere on the other hand showed increased amplitude at 0.25 Hz at day 2 after stroke in both GCaMP and hemodynamics. Fig. 5d shows the area under the curve in the frequency range of 0.1–0.3 Hz, where the largest increase was observed. The increase in oscillatory amplitude at 0.25 Hz, which is typically higher than normal for hemodynamics, could be a result of increased vasomotion. Evidence from prior work in human laser doppler flowmetry and magnetoencephalography (MEG) has suggested that stroke affected arterioles showed elevated oscillatory amplitudes (Laaksonen et al., 2013; Goltsov, 2017).

We then asked if this increase in power of the GCaMP, in the contralesional hemisphere, and hemodynamic signal, in both hemispheres, was uniform across the hemispheres or specific to any distinct brain region. Fig. 5e shows spatial maps of the average power spectrum for GCaMP and HbO for one typical mouse. We clearly see increased amplitude in GCaMP in the contralesional hemisphere and increased

overall amplitude in HbO at day 2 and week 1 compared to pre-stroke. Surprisingly, the increase in GCaMP activity appeared specific to the contralesional forelimb region, while the increase in HbO appeared global. When validated across all mice (Fig. 5f), we observed a significant increase in GCaMP oscillatory dynamics within only the contralesional forelimb and not the rest of the contralesional hemisphere. The HbO signal on the other hand showed increases across all regions, the ipsilesional and contralesional forelimb and non-forelimb areas. There was also a decrease in the GCaMP signal within the ipsilesional forelimb region in the chronic phase, which is likely due to loss of neurons within that region.

2.5. Photothrombotic stroke disrupts resting state interhemispheric functional connectivity only in the very acute phase

Stroke has also been known to affect functional connectivity across large scale brain networks (Grefkes and Fink, 2011; Grefkes and Fink, 2014). To address the possibly differential effects of stroke on calcium and hemodynamic global brain dynamics we asked whether resting state functional connectivity (RSFC) showed similar dynamics during the recovery phase. Prior work in healthy animals has showed that at low (0.009–0.08 Hz) and high (0.08–0.4 Hz) frequency bands, which are typically used in BOLD fMRI and functional connectivity IOSI studies, functional connectivity structures between GCaMP and HbO were in high agreement (Wright et al., 2017). But as applications of hemodynamic RSFC are extended into the stroke field it is not only important to understand the underlying physiology that those signals represent but also what aspects of connectivity are altered and are sensitive measures for the stroke (Bauer et al., 2014; Chung, 2021).

To that end, we looked at various aspects of RSFC in the low and high frequency bands across the GCaMP and HbO maps. First, we assessed connectivity of the ipsilesional forelimb area to the contralesional hemisphere (Fig. 6a). In healthy pre-stroke animals, seed-based forelimb connectivity maps were consistently normal when compared to prior work, while acute stroke showed alterations in forelimb connectivity to the contralesional hemisphere (Chung, 2021; Kura et al., 2018; Xie, 2020). Fig. 6a(i) shows the forelimb connectivity maps for GCaMP at pre-stroke, day 2, and week 4 in the low frequency band. We then quantified the differences between pre-stroke and each post-stroke time point by calculating the proportional area of the cortex above a certain correlation coefficient threshold that ranged from 0 to 0.9 (Fig. 6a(ii)). A slight decrease in connectivity was observed in the GCaMP map and a large decrease was observed in HbO at 2 days post-stroke (Fig. 6a(ii), Supplementary figure 10a). HbO continued to show reduced forelimb connectivity at all time points after stroke at specific thresholds (Supplementary figure 10a), however, GCaMP connectivity appeared largely restored at later time points. A Dice similarity index was calculated between the GCaMP and HbO maps across all thresholds, which showed a deviation in similarity only at day 2 after stroke, while maps were consistent at all other time points (Fig. 6a(iii), Supplementary figure 10a). A similar approach was used for calculating interhemispheric connectivity, global connectivity, and contralesional forelimb intrahemispheric connectivity as well as all measures in the higher frequency
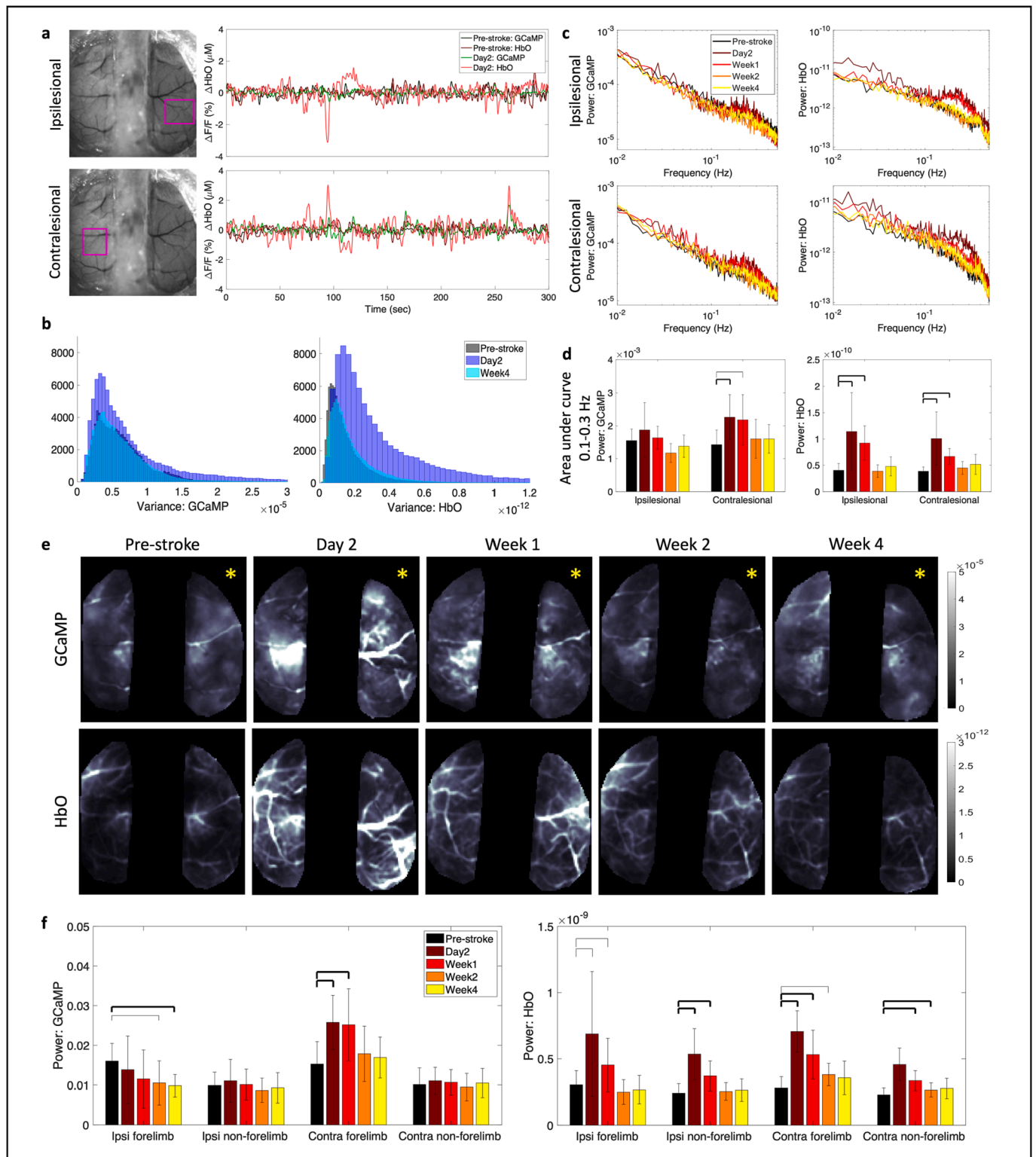
Fig. 5. Global brain oscillations following stroke. (a) Raw time traces of filtered (0.009–0.4 Hz) calcium and hemodynamic signals before and 2 days after stroke within the ipsilesional (top) and contralesional (bottom) hemispheres in ROI marked with pink box. Note the increase in amplitude of HbO in both hemispheres at day 2 and increase in GCaMP amplitude only in the contralesional hemisphere. (b) Histogram of variance in the mean signal, after global signal regression, for GCaMP (left) and HbO (right) at pre-stroke, day 2, and week 4. (c) Frequency spectrum of the power of the GCaMP (left) and HbO (right) signal in the ipsilesional (top) and contralesional (bottom) hemispheres. (d) Area under the curve within 0.1–0.3 Hz frequency band. Thick bars: $p < 0.01$, thin bars: $p < 0.05$. (e) Spatial maps of average power across 0.009–0.4 Hz frequency band for GCaMP (top) and HbO (bottom) at each time point. Yellow asterisk indicates the stroke hemisphere. (f) Mean power assessed in each hemisphere within the forelimb and non-forelimb areas. A two-sample *t*-test was run for all statistical tests. Thick bars: $p < 0.01$, thin bars: $p < 0.05$. (For interpretation of the references to colour in this figure legend, the reader is referred to the web version of this article.)
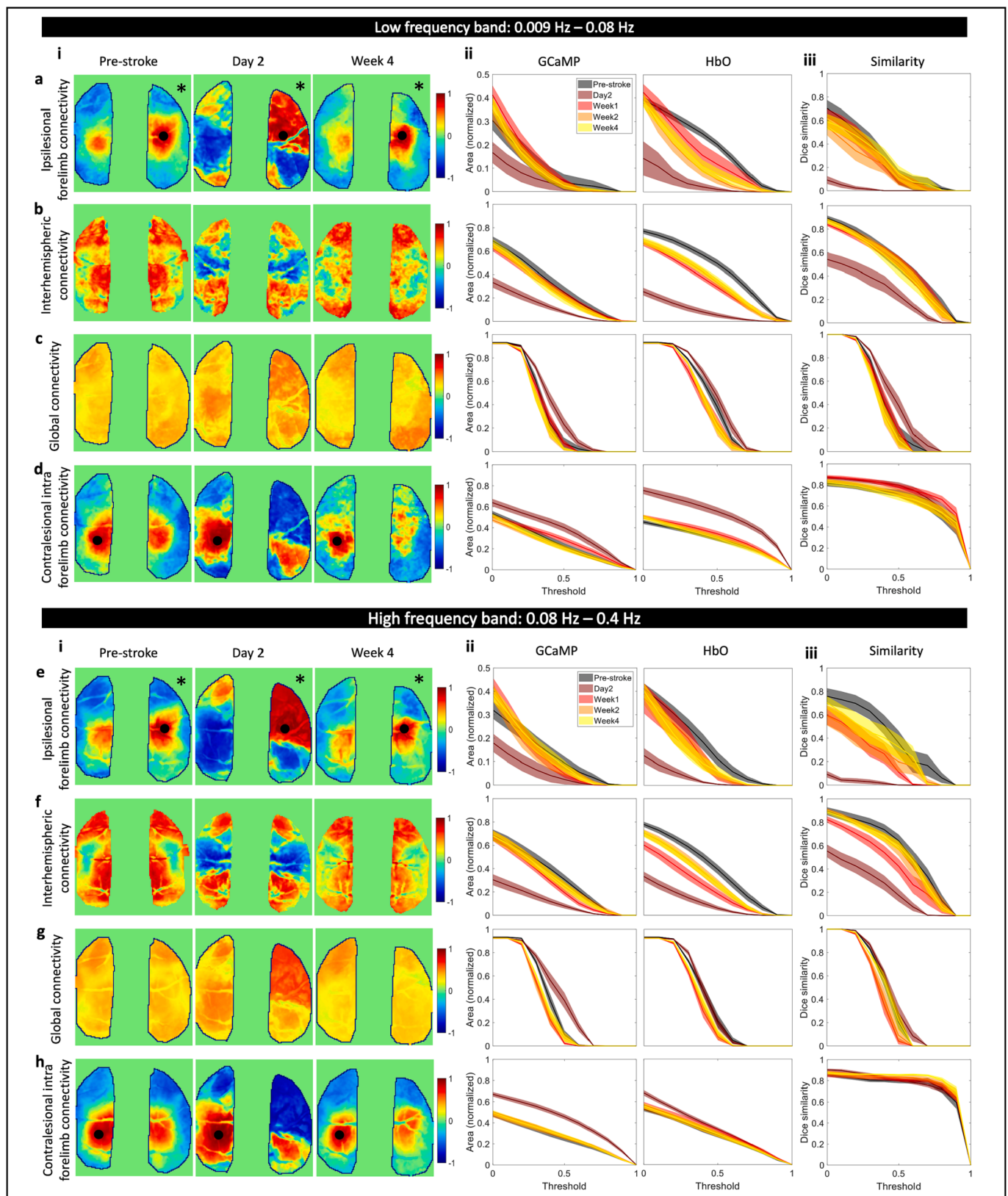
Fig. 6. Global brain network dynamics assessed with RSFC. Spatial maps of ipsilesional forelimb connectivity (a(i),e(i)), interhemispheric connectivity (b(i),f(i)), global connectivity (c(i),g(i)), and contralesional forelimb connectivity (d,h) in the low frequency band (a,b,c,d) and the high frequency band (e,f,g,h) at pre-stroke, day 2, and week 4. Proportional area of cortex over threshold for GCaMP and HbO at each time point for ipsilesional forelimb connectivity (a(ii),e(ii)), inter-hemispheric connectivity (b(ii),f(ii)), global connectivity (c(ii),g(ii)), and contralesional forelimb connectivity (d(ii),h(ii)) in the low frequency band (a,b,c,d) and in the high frequency band (e,f,g,h). Dice similarity coefficient for overlap between area covered by GCaMP and HbO for ipsilesional forelimb connectivity (a(iii),e(iii)), interhemispheric connectivity (b(iii),f(iii)), global connectivity (c(iii),g(iii)), and contralesional intrahemispheric forelimb connectivity (d(iii),h(iii)) at all time points in the low frequency band (a,b,c,d) and the high frequency band (a,b,c,d). Black asterisk indicates the stroke hemisphere.

band. Trends across time points and thresholds for all measures were largely similar in both frequency bands. There was a significant drop in interhemispheric connectivity at 2 days in both GCaMP and HbO, which was restored at later time points in GCaMP but continued to persist, to a lesser extent, in HbO until week 1 (Fig. 6b,f). Surprisingly there was a small but significant increase in global connectivity at day 2 in GCaMP (Fig. 6c,g, Supplementary figure 10c). Spontaneous recovery over four weeks resulted in reestablishment of global connectivity networks in both GCaMP and HbO. Since we observed increase in the calcium power within the contralesional hemisphere (previous section) we also asked whether contralesional forelimb connectivity was altered. We observed a significant increase in contralesional forelimb connectivity within the contralesional hemisphere at day 2 after stroke (Fig. 6d,h, Supplementary figure 10d). This suggests that increases in the power of the calcium signal within the contralesional forelimb was associated with an increase in its functional connectivity to other regions of the brain. The increase observed in the global connectivity index could be due to this increased connectivity of the contralesional forelimb.

From these data we extrapolate that connectivity of both the impaired and unimpaired forelimb and interhemispheric connectivity for both GCaMP and HbO were reliable measures to indicate stroke, given our photothrombotic model, at day 2. Disruptions to interhemispheric connectivity persisted until week 1 after stroke, however other metrics assessed were indistinguishable from pre-stroke. While global connectivity provides a concise method as a seed-independent approach of functional connectivity, in our case it was a weaker metric for following the stroke recovery process.

2.6. Correlating acute phase cortical metrics to long-term behavior outcomes

To enable translation of the cortical measures investigated in this work to potentially clinically relevant long-term behavioral outcomes, we measured forelimb performance through the cylinder asymmetry test before stroke and at each imaging time point after stroke. Photothrombotic stroke to the forelimb somatosensory area led to deficits in the use of the impaired forelimb (Fig. 7a). Mice used their impaired forelimb 50 % less than baseline in the first week following stroke, however, over time with spontaneous recovery, mice showed a significant increase in the use of the impaired forelimb by week 4 compared to day 2 (Fig. 7a, Supplementary table 1). An important factor in human strokes that is often missed in animal models is the variability in the extent of damage and impairment caused by the stroke. The extent and location of the damage due to stroke as well as the early spontaneous recovery mechanisms play a significant role in long-term outcome (Sharma and Cohen, 2012; Cramer, 2008; Angels Font et al., 2010). A number of early biomarkers that might have potential as indicators of behavioral outcome are under active investigation in both humans and in animal studies (Boyd et al., 2017; Stinear, 2017). While it would be ideal to introduce a controlled level of variability in terms of ischemic damage into animal models to study variable recovery and to identify biomarkers that indicate recovery, such a method of stroke induction does not yet exist that also meets all the other criteria for a physiological stroke, such as preventing the use of anesthesia during stroke induction. Our optimized photothrombotic model introduces uncontrolled variability in the stroke size (Supplementary Fig. 1) that mimics human variability to some extent and allows correlation of behavioral outcome
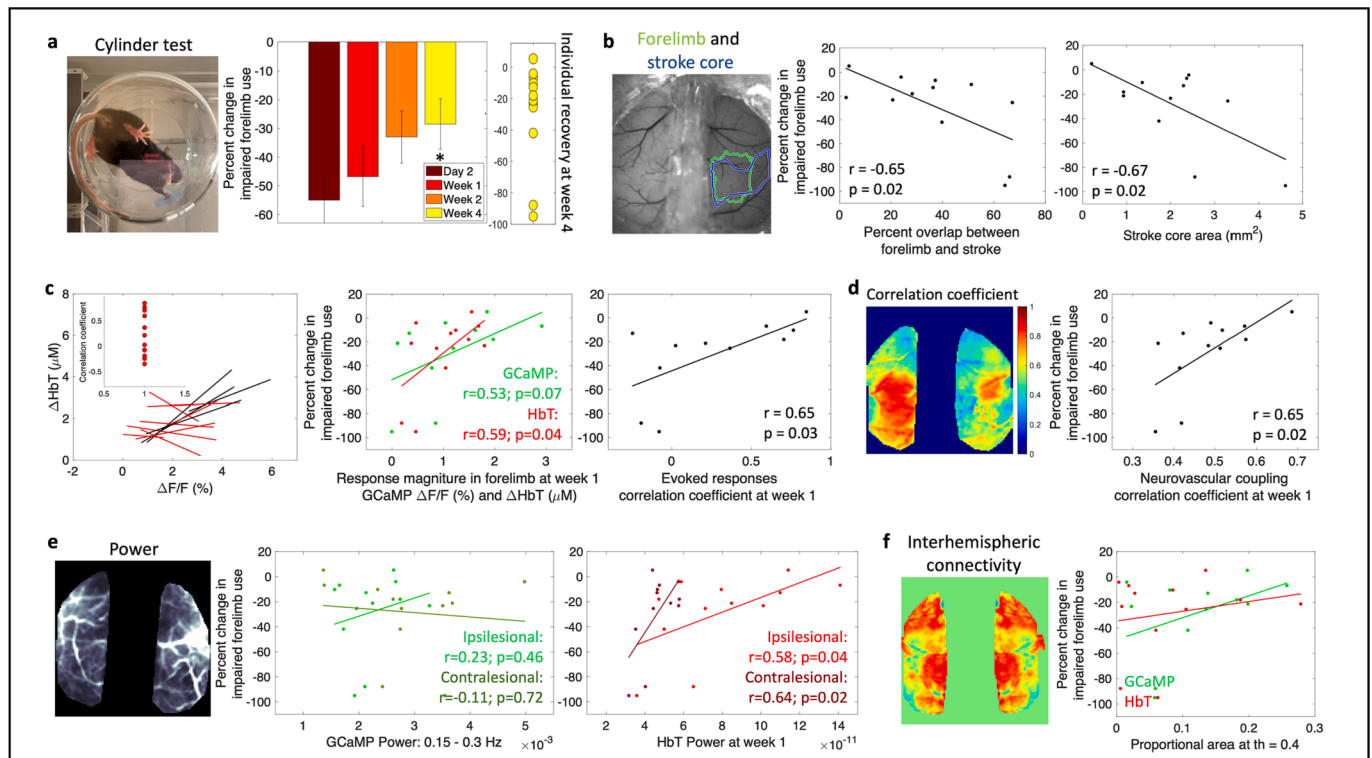

Fig. 7. Correlating cortical metrics to behavior outcomes. (a) Forelimb asymmetry, assessed with the cylinder test, calculated as a change in impaired forelimb use from pre-stroke, right: recovery of individual mice at week 4. (b) Left: reference image showing outlines of pre-stroke forelimb region and stroke core at 1 week, middle: correlation between overlap of forelimb and stroke with forelimb asymmetry at week 4, right: correlation between stroke area and forelimb asymmetry at week 4. (c) Left: correlation of evoked responses of GCaMP and HbT, middle: correlation between response magnitude at week 1 for GCaMP and HbT with forelimb asymmetry at week 4, right: correlation between the correlation coefficient of evoked responses at week 1 and forelimb asymmetry at week 4. (d) Left: correlation coefficient between measured HbT and HbT predicted by convolving GCaMP and IRF, right: correlation between neurovascular coupling correlation coefficient at week 1 and forelimb asymmetry at week 4. (e) Correlation between power of GCaMP and HbT in frequency band 0.15–0.3 Hz in the ipsilesional and contralesional hemispheres and forelimb asymmetry at week 4. (f) Correlation between resting state interhemispheric connectivity and forelimb asymmetry at week 4.

to cortical biomarkers. The right panel of Fig. 7a shows the extent of recovery in forelimb asymmetry for individual mice at week 4. In this section we outline how cortical measures obtained in all the previous sections correlate to these variable long-term behavioral outcomes.

First, since the cylinder test is sensitive to forelimb use, we tested whether the extent of forelimb area that was damaged due to stroke predicted behavioral outcomes. We calculated the percent overlap between the pre-stroke forelimb region and the stroke outline obtained at 1 week after stroke from SFDI (Fig. 7b). There was a significant negative correlation indicating that worse behavior outcomes correlated with a larger portion of the forelimb activation area being damaged by the stroke. In addition to overlap with forelimb, behavior outcomes were significantly negatively correlated with extent of initial injury, which was the stroke core defined by SFDI. This indicated that extent of injury was predictive of long-term behavioral outcomes. While the percent overlap between forelimb area and stroke core did not show significant correlations with functional measures of NVC disruptions, the stroke core area alone showed a significant negative correlation with NVC correlation coefficient at week1 (Supplementary figure 11c). However, stroke core area was not predictive of NVC recovery at week4 (Supplementary figure 11d). Additionally, stroke core area showed weak negative correlations to other functional measures at week1 but were not significant (Supplementary figure 11). These data suggest that the stroke size might be indicative of and a useful biomarker for understanding the extent of NVC disruptions in the subacute phase but does not reliably predict NVC recovery in the chronic phase.

We next asked whether functionality in the surviving portion of the forelimb region promoted behavioral recovery. Here, we calculated the magnitude of responses within the original forelimb region for GCaMP and hemodynamics at week 1. Both GCaMP and hemodynamics showed trends towards a positive correlation between response magnitude and better outcomes, with only the HbT showing a significant correlation (Fig. 7c). The correlation coefficients obtained from the magnitude of evoked responses between GCaMP and HbT at week 1 during forelimb stimulation significantly correlated with behavioral outcomes (Fig. 7c, data from Fig. 3). Next, we assessed the relationship between acute neurovascular coupling and behavior outcomes. The correlation co-efficients obtained from the neurovascular coupling HRF model between the measured and estimated HbT at week 1 also showed a significant correlation with behavioral outcomes implying that preserved or improved neurovascular coupling at week 1 might be indicative of better long-term recovery (Fig. 7d). We performed similar calculations with the global brain metrics of power of the signal and interhemispheric connectivity from RSFC. Average power was calculated within the narrow frequency band (0.15–0.3 Hz) for both GCaMP and hemodynamics and separated into ipsilesional and contralesional hemispheres. While GCaMP did not show any trends with behavior, acute hemodynamic oscillations showed strong positive trends with behavior outcomes (Fig. 7e). Specifically, increased power in the HbT signal of the contralesional and ipsilesional hemispheres in the acute phase of stroke significantly correlated with behavior outcomes. Interhemispheric connectivity at week 1, or any other RSFC metric, did not show any correlations with long-term behavior outcomes, further implying that RSFC might not be a sensitive metric for targeted photothrombosis.

Overall, we have identified several cortical metrics within the acute phase of stroke recovery that had the potential to delineate animals with better spontaneous recovery versus animals that had poorer recovery. While these analyses are suggestive of potential biomarkers for recovery, a limitation is that our dataset includes only two animals that showed poor recovery at week 4. Increased spontaneous recovery is likely a consequence of the photothrombotic stroke model that targets a single pial arteriole. Further investigation is needed with a stroke model that introduces controlled variability to draw conclusions about biomarkers for recovery.

3. Discussion

While functional neuroimaging has potential for monitoring patients and guiding treatment in the acute and chronic phases of stroke recovery, the interpretations of these signals and their reliability as a neural correlate is still under active investigation. In this study, we used an animal model of stroke, which was optimized for high clinical relevance, to investigate the relationships between neural activity, assessed with a fluorescent calcium indicator, and cerebral blood volume, assessed with changes in oxy and deoxy hemoglobin, during longitudinal stroke recovery. We showed that neurovascular coupling was preserved and mimicked healthy conditions in the chronic phase of stroke recovery. Neurovascular uncoupling was observed in the acute phase of stroke recovery primarily in the affected hemisphere, and early recoupling and recovery of cortical function within the preserved forelimb region and peri-infarct zone was an indicator of better recovery. Additionally, we showed that acute stroke leads to increased global brain oscillations, which show distinct spatial characteristics in GCaMP and hemodynamics. Specifically, neural oscillations were observed in the homotopic region of the contralateral hemisphere whereas hemodynamic oscillations were observed across the whole window in both hemispheres. We have combined several complementary techniques to study NVC across the whole brain longitudinally and have revealed useful insights in the evolution of NVC and brain oscillations during stroke recovery and its associations with behavioral recovery.

The results from this study show that we were able to combine an optimized photothrombotic stroke model with wide-field assessment of neurovascular coupling to study stroke recovery across a cohort of animals with variable recovery. The results presented have several implications for the interpretations of hemodynamic signals in terms of the underlying physiology in both pre- and post-stroke. In the healthy brain we showed that with simultaneous multi-modal imaging of neural calcium activity and hemodynamics we can track subtle differences in sensory evoked response dynamics on a trial-by-trial basis. This allowed us to correlate intra-animal changes to evoked responses across the cohort and at each time point after stroke. We correlated each animal's responses individually due to the variability in the extent of ischemic damage among animals introduced by our stroke model. We found that there was a significant loss in correlation between evoked calcium and hemodynamic responses in the acute phase at day 2 and week 1. Correlation was reestablished in most animals by week 4 signifying spontaneous recovery and improved behavior. A small number of animals continued to show loss of correlation between evoked calcium and hemodynamic responses across both the acute and chronic time points and these animals were associated with poor behavior outcomes. There was also a significant positive trend between correlation of evoked responses, specifically between calcium and HbT, at week 1 and behavior outcomes at week 4 across all mice. Taken together with the significant correlation between early HbT response magnitudes within preserved forelimb and long-term behavior, this implies that early recovery of hemodynamic responses, HbT in particular, might be indicative of better outcomes.

To quantitatively describe neurovascular coupling, we predicted hemodynamics from calcium activity using linear least-squares deconvolution as has been done previously (Ma, 2016; Lake, 2020). Similar to previous reports, the measured calcium signal convolved with a calculated HRF kernel predicted the hemodynamic signal to a high degree in healthy animals. There was a higher correlation within sensory regions of both hemispheres compared to more frontal or posterior regions, likely due to sensory stimulation driving cortical activity within somatosensory cortex and strengthening the observed neurovascular coupling signal. The characteristic shape of the HRF was altered after acute stroke, which also corresponded with a significant decrease in the ability of the model to predict hemodynamics within the affected hemisphere. The correlation when using the pre-stroke "healthy" HRF was significantly lower than the correlation when using the time-point

specific post-stroke HRF. This indicates that while the model post-stroke was finding the best fit, the resulting HRF was not necessarily similar to the expected neurovascular coupling model under healthy conditions. Using the expected neurovascular coupling model yielded significantly worse correlations. These results suggest that the neurovascular coupling model established in healthy animals was not representative of post-stroke acute phase dynamics and that the observed hemodynamic response might not be an accurate representation of the underlying physiology. However, it must also be noted that the model assumption of a linear relationship might not hold true after stroke, and the hemodynamic response might be better predicted with an altered non-linear model. Weak neural signals and potentially altered calcium indicator dynamics due to cell stress make it difficult to interpret the uncoupling observed in the acute phase. For instance, we observe sharp peaks in the HRF at t = 0 in Fig. 4f, which might be due to higher crosstalk between calcium and hemodynamics. Additionally, global oscillations at 0.1–0.3 Hz in the acute and sub-acute phases of stroke might influence the deconvolution model and impact the accuracy of the linear assumption in determining the HRF. Further investigation is needed to understand the dynamics of genetically encoded calcium indicators in stroke to aid in developing better methods to unmix the signals as well as develop new NVC models if modified in the acute phase. Nevertheless, uncoupling in the acute phase observed in this study is also supported by uncoupling observed in prior studies using electrode recordings (He, 2020) and might suggest that functional neuroimaging might not represent the underlying neural activity and care must be taken when interpreting the results in the acute phase of stroke recovery. However, we see restoration of neurovascular coupling, in accordance with the linear model, in the chronic phase of recovery. We observed reestablishment of the expected HRF shape and improvement in the ability of the model to predict hemodynamics, specifically in the peri-infarct region. Moreover, the pre-stroke HRF was able to predict hemodynamics to a high degree in the chronic phase of recovery indicating that the restored neurovascular coupling resembles healthy conditions. This also suggests that functional neuroimaging might be faithfully representing the underlying neurophysiology in the chronic phase.

In addition to local changes to evoked responses and neurovascular coupling alterations within the affected hemisphere, stroke is known to have an impact on global network dynamics such as contralateral and subcortical connectivity (Grefkes and Fink, 2014). We found that there was an increase in the overall oscillatory amplitude of cortical signals in both calcium and HbT in the acute phase, which was resolved in the chronic phase. The increase in oscillations of the calcium signal appeared to be specific to the contralesional forelimb region, while the increase in hemodynamic oscillations was global across all vessels and both hemispheres. A prior study conducted with laser doppler flowmetry showed increased oscillations within stroke affected arterioles and suggested increased vasomotion as the cause (Goltsov, 2017). Other studies have also showed increases in brain oscillations in stroke and traumatic brain injury (Laaksonen et al., 2013; Rabiller et al., 2015; Huang et al., 20202020). Vasomotion, which is the oscillating tone of blood vessels independent of heart rate or breathing, is tightly regulated, and maintained by various compartments of the neurovascular unit (Intaglietta, 1991; Intaglietta, 1990). Vascular autoregulation is impaired after stroke and ionic imbalances in neural, astroglial, and endothelial cells could result in dysregulation of vasoactive molecules and ions and therefore vascular tone (Kunz and Iadecola, 2009; Girouard and Iadecola, 2012). On the other hand, we also observed increases in power of GCaMP in the contralesional forelimb. Prior work has shown that stroke leads to increases in brain excitability and disruption of the interhemispheric inhibition through the corpus callosum (Carmichael, 2012; Joy and Carmichael, 2021; Bütefisch et al., 2003). This could reduce the inhibitory effects that the two hemispheres exert on each other, which could increase excitability within the contralesional hemisphere. There is also evidence of thalamic disinhibition within minutes of ischemic stroke that can unmask ipsilateral pathways

(Mohajerani et al., 2011). The excitability of thalamocortical pathways contralateral to the stroke may be enhanced because of downregulation on interhemispheric thalamic inhibition. Surprisingly, we found that increased oscillations in the hemodynamic signal in the contralesional hemisphere during the acute phase was correlated with improved behavior outcomes. Prior work has shown that stimulation of activity within the gamma frequency band improved cerebral blood flow, decreased infarct volume, and improved motor behavior, suggesting that modulation of cortical oscillatory dynamics may serve as a target for neuroprotection (Balbi, 2021). Other studies have also shown that increased brain oscillations and excitability promoted recovery in stroke as well as other neurological disorders and suggest its possible use as a biomarker for recovery (Rabiller et al., 2015; Carmichael, 2012; Joy and Carmichael, 2021; Adaikkan et al., 2019). A meta-analysis on activation data from over 50 neuroimaging experiments have shown enhanced activity in the homotopic region of the contralesional hemisphere in the acute phase after stroke (Rehme et al., 2011; Rehme et al., 2012). This enhanced activity appears as spontaneous and synchronous neural activity and has been shown to be a signal for axonal sprouting and reorganization (Carmichael and Chesselet, 2002). Taken together with this evidence, we could hypothesize that spontaneous increases in oscillatory activity that we observed in hemodynamic activity might play a role in promoting recovery mechanisms. These vascular oscillations are most likely driven by slow frequency variations in the power of gamma oscillations that are known to drive the vascular oscillations associated with resting-state functional connectivity in the same frequency range of ~0.1 Hz (Mateo et al., 2017). These oscillations are possibly driven by underlying neural activity at frequencies higher than we can measure with our current acquisition rates of 5 Hz.

A growing number of studies are now using RSFC to assess spatiotemporal correlations in spontaneous hemodynamic signals across different brain regions in healthy and diseased states. In the healthy brain, hemodynamic signals have been found to be bilaterally correlated and synchronized temporally in functionally distinct brain regions and represent the connectivity of underlying intrinsic neural fluctuations (Ma, 2016; Kura et al., 2018; White et al., 2011). RSFC has also been used as a sensitive assay to monitor progression of stroke and hemorrhage with the assumption that the altered connectivity represents the altered neural state (Bauer et al., 2014; Chung, 2021). In this study we show that RSFC of spontaneous calcium activity and hemodynamics show similar trends after stroke, validating prior assumptions. Forelimb and interhemispheric connectivity were disrupted significantly in the very early acute phase and was resolved within week 1 in both calcium and hemodynamics. Moreover, we found that RSFC measures were not predictive of behavioral outcome. This could be because global brain connectivity is more robust to small strokes caused by targeted photothrombosis to the forelimb. A prior RSFC study also showed that somatosensory connectivity was not predictive of behavior but motor and retrosplenial cortices might be better predictors (Bauer et al., 2014). Due to our window preparation procedure and headbar design for multimodal optical access we were limited in the field-of-view to mainly the somatosensory region and were unable to capture connectivity to other brain regions to their full extent. It is also possible that more sensitive analyses are needed for RSFC to serve as a metric for stroke outcome. For instance, we did not remove periods of animal movement from the analysis. We also tested whether increases in power of the calcium activity within the contralesional forepaw was associated with increased functional connectivity through RSFC. We found that intra-contralesional hemisphere connectivity was significantly increased at day 2. This suggests that increased excitability within the contralesional forepaw might result in its increased functional connectivity to surrounding regions as well as the ipsilesional peri-infarct, as seen from the spatial maps of connectivity. Further investigation is needed to understand the link between excitability and functional connectivity and its impact on recovery.

An important factor to note in our study is that we measure calcium

dynamics from only excitatory cells. We know, from decades of prior work, that both excitatory and inhibitory cells have important and distinct roles to play in maintaining cortical balance (Isaacson and Scanziani, 2011). Additionally, a number of other cell types, such as astrocytes and pericytes, and modulators are involved in regulating blood flow to meet the metabolic demands of the brain (Kleinfeld, 2011; Hamel, 2006; Attwell et al., 2010). We also know that these different cell types are impacted differently after stroke (Moskowitz et al., 2010; Lo et al., 2005; Lo et al., 2003). While the current study used mice with labelled excitatory neurons, the same imaging platform and experimental design can be used to investigate the contributions of other cell types, such as inhibitory cells and glia, to alterations in neurovascular coupling after stroke. Additionally, calcium dynamics assessed with GCaMP6f has been validated to be a reliable measure of neural activity, however, it is still not a direct measure of neural electrical activity. Fast neural dynamics or sub-threshold dynamics may be missed in calcium imaging since the dynamics of calcium are much slower than action potentials or local field potentials (Chen et al., 2013; Luo et al., 2018; Xu et al., 2017). Although performing similar experiments while capturing local field potentials would allow us to assess neural activity directly and provide a higher temporal resolution, we do not believe that using GCaMP has affected our assessment of neurovascular coupling as all our experiments are performed at a temporal resolution higher than what is needed for hemodynamics assessment (Ma, 2016). However, using a genetically encoded reporter of activity, such as GCaMP, has limitation in studies of cellular stress and cell death. The expression and activity of the reporter has been suspected to be affected by ischemia and could therefore confound our interpretations of neural activity. We expect this effect to have the largest impact on analyses performed in the acute phase within the core region of the stroke and requires further work to validate the GCaMP signal's true origins at day 2 and week 1 following stroke. It is unlikely that this impacts analyses performed in the peri-infarct region or the contralesional hemisphere as the stroke core is defined based on time-point specific SFDI measures, which is capturing the extent of cellular stress and damage. Electrophysiology recordings of local field potential and spiking activity performed by He et al. (He, 2020) also show disruptions to NVC in the acute phase, further confirming that the data in this paper in the acute phase is not purely an artifact of low GCaMP signals.

In summary, we have combined a mouse model and imaging technique that can assess wide-field neurovascular coupling longitudinally after stroke across both hemispheres of the brain. This combination of tools can be used to assess the contributions of individual compartments of the neurovascular unit to neurovascular coupling before and after brain injury. Here we show the effects of stroke on excitatory and hemodynamic activity during the acute and chronic phases of stroke recovery. Our exploratory results suggest that acute stroke leads to neurovascular uncoupling, implying that functional neuroimaging by fMRI and fNIRS might not fully represent the underlying neural activity and one needs to use caution when interpreting the results. Neurovascular coupling is restored in the chronic phase, suggesting that these functional neuroimaging methods more faithfully represent the underlying neural activity chronically. Moreover, early recovery of neurovascular coupling and increased power of brain oscillations were predictors of better long-term behavioral outcomes.

4. Materials and methods

4.1. Experimental design

All experiments and animal procedures were approved by the Boston University Institutional Animal Care and Use Committee and were conducted following the Guide for the Care and Use of Laboratory Animals. All animals used in this study were adult Thy1-GCaMP6f mice (Jackson Labs, strain code: 025393, C57BL/6J-Tg(Thy1-GCaMP6f) GP5.17Dkim/J)). Mice were implanted with bilateral cranial windows,

one window on each of the hemispheres, and allowed to recover for two weeks. Following recovery, mice underwent a habituation training in an imaging cradle to get accustomed to the imaging setup and environment at least 10 days prior to imaging sessions. In addition to cradle habituation, animals were habituated on sensory air puff stimulation for two sessions before imaging sessions were performed. All imaging sessions were performed in awake head-fixed animals. Pre-stroke control measures were obtained one week prior to stroke and photothrombotic stroke was performed on Day0 of the experiment. Following photothrombosis, mice were imaged longitudinally at Day2, Week1, Week2, and Week4 to span acute, subacute, and chronic phases of stroke recovery. To correlate the cortical measures to a behavior metric, forelimb asymmetry was measured using the cylinder test at each of the imaging time points. The timeline of experiments is outlined in Fig. 1a and details of methods are elaborated in the following subsections.

4.2. Animal preparation

A bilateral cranial window exposing both hemispheres of the brain was implanted in all mice to determine the effect of stroke on both the ipsilesional and contralesional hemispheres. The surgical procedure for implantation of bilateral cranial windows followed a similar procedure to unilateral windows that has been previously described (Sunil et al., 2020). Briefly, mice were injected with Buprenorphine subcutaneously 1 h prior to the start of surgery. During surgery, mice were anesthetized with isoflurane (3 % at induction and 1–1.5 % for maintenance with 1 L/min oxygen) and body temperature was maintained at 37 °C. Respiratory rate and toe pinch were used to monitor the depth of anesthesia throughout the surgical procedure. After incision of the scalp, a round aluminum head post, 12 mm in diameter, was attached to the intact skull with dental acrylic. A craniotomy was the performed on one hemisphere of the brain in order to remove the skull. A half-skull-shaped curved glass (modified from Crystal Skull (Kim, 2016), LabMaker, Germany) was used to cover the surface of the brain and then sealed with optical glue and dental acrylic. The craniotomy and glass procedure were repeated on the other hemisphere of the brain in order to create a bilateral cranial window implant. Recovery procedures were followed according to the guidelines provided by Boston University. After a two-week recovery period from surgery, mice were trained to remain head-fixed for up to 90 min for approximately 10 days. All experiments are done in awake head-fixed mice.

4.3. Instrumentation

The instrumentation used in this work has been described in our prior publications (Sunil et al., 2020; Sunil, 2021). The instrument is a multimodal system that can perform fluorescence calcium imaging, intrinsic optical signal imaging (IOSI), laser speckle contrast imaging (LSCI), spatial frequency domain imaging (SFDI), and targeted photothrombosis in vivo. The body of the system consists of a 2X objective with an NA of 0.1 to collect emitted light. A 640 nm dichroic mirror is used to split the emitted light into two arms: 1) light below 640 nm is reflected into the fluorescence, IOSI, and SFDI arm, and 2) light above 640 nm is transmitted into the LSCI arm. The light emitted into the IOSI arm passes through a 500 nm long pass filter and a 650 nm short pass filter before being focused onto a sCMOS camera using a 200 mm infinity corrected tube lens. The light transmitted into the LSCI arm is passed through a 785 nm bandpass filter, a polarizer, and an iris, and focused onto a CMOS camera using a 200 mm infinity corrected tube lens. Excitation for calcium and IOSI imaging is provided by 3 collimated LEDs (470 nm, 530 nm, and 625 nm) located obliquely above the cranial window. Excitation for LSCI imaging is provided by a 785 nm laser diode also located obliquely above the cranial window. Illumination for SFDI is provided by a 530 nm LED that is collimated and projected onto a digital micromirror device (DMD). The DMD spatially modulates the light at desired frequencies, and the pattered illumination

is projected onto the cranial window. A polarizer in the illumination and imaging paths are used to cross polarize the light to reduce specular reflections. The photothrombosis arm of the setup, which consists of a 520 nm laser diode and scan lenses to control the beam size on the surface arteriole, is integrated into the IOSI arm, and photothrombosis is performed through *epi*-illumination. A National Instruments NI-DAQ card and custom Matlab scripts are used to trigger and synchronize camera acquisition and LED excitation.

4.4. Spatial frequency domain imaging

To capture the spatial extent of the stroke core longitudinally as well as to aid in fluorescence correction for hemodynamic crosstalk, SFDI was performed pre-stroke and at each time point post-stroke. The instrumentation, acquisition, and analysis to obtain absorption and scattering coefficients of the tissue have been described previously and summarized above (Sunil, 2021). Mice were placed in the imaging cradle and allowed to habituate for 10 min prior to the start of imaging for every session. Spatially varying sinusoidal patterns were projected onto the cranial window by a digital micromirror device (DMD), and the reflected light was imaged by a sCMOS camera. Two spatial frequencies (0 and 0.4 mm^{-1}) were projected at three phases (0, 120, and 240 deg). The acquired images were processed offline using a custom Matlab script. The intensity at each spatial frequency was demodulated and calibrated to a reference phantom to obtain the diffuse reflectance using:

$$M_{AC}(x_i, f_x) = \frac{2^{1/2}}{3}\left[(I_1 - I_2)^2 + (I_2 - I_3)^2 + (I_1 - I_3)^2\right]^{1/2}$$

$$R_d(x_i, f_x) = \frac{M_{AC}(x_i, f_x)}{M_{AC,ref}(x_i, f_x)}.R_{d,ref}(f_x)$$

as described previously (Cuccia et al., 2009). M_{AC} is the demodulated AC component and I_1, I_2, and I_3 are the reflected intensity images at the three phases for each spatial frequency. M_{AC} images were then calibrated to the reference phantom to obtain the diffuse reflectance R_d. A two-frequency lookup table was generated by Monte Carlo simulations at the two frequencies used for imaging from which absorption and scattering coefficients were extracted. Scattering coefficients were used to determine infarct area and stroke properties, such as the core, periinfarct, and healthy tissue, as outlined below. SFDI was also used in the correction of GCaMP for hemodynamic crosstalk. The absorption and scattering properties obtained at each time point post-stroke were used to run a Monte Carlo simulation, as described below, to determine the pathlength of light travelled in tissue. This pathlength is then used in the correction algorithm to scale the GCaMP signal, based on the time-varying changes in hemodynamic absorption, for accurate estimation of calcium dynamics.

4.5. Simultaneous hemodynamic and calcium imaging

To evaluate local and global changes in neurovascular coupling post-stroke simultaneous measures of hemodynamic and neural activity were obtained during forelimb sensory stimulation and resting state. The instrumentation, task setup, and data analysis pipeline for measuring cortical hemodynamics has been outlined previously (Sunil et al., 2020). Fig. 1a shows a simplified schematic of the imaging setup. Intrinsic optical signal imaging was used to assess changes to oxy and deoxy hemoglobin, HbO and HbR respectively, for the hemodynamic measure, and fluorescence GCaMP imaging was performed to assess changes in calcium dynamics as a measure of neural activity. The cortical windows were illuminated sequentially with 470 nm, 530 nm, and 625 nm LEDs (MXL3-C1, Thorlabs, X is the center wavelength), where the 470 nm LED was used for GCaMP excitation and the 530 nm and 625 nm LEDs were used for calculations of oxy and deoxy hemoglobin. A 500 nm long pass filter (FELH0500, Thorlabs) placed along the detection path blocked out

any GCaMP excitation light. Images were collected by a sCMOS camera (Hamamatsu ORCA-Flash 4.0 V3) at 15 Hz, 5 Hz per wavelength, with an exposure time of 50 msec. For resting state, spontaneous activity was obtained for 10 min. For sensory stimulation, two imaging session were performed at each time point pre- and post-stroke, one where the contralateral (affected) forelimb was stimulated and the second where the ipsilateral (unaffected) forelimb was stimulated. Each stimulation session consisted of 20 trials where each trial was obtained in a block-design fashion and consisted of 5 s of baseline, followed by 5 s of 3 Hz air-puff stimulation, followed by 20 s of recovery. Air puffs, which were generated by a piezoelectric generator that was synchronized to the imaging instrument using the NI-DAQ card, were delivered through a glass pipette positioned 2 cm in front of the forelimb. A custom Matlab script was used to synchronize and trigger the sequential LEDs, camera acquisition, and air puff stimulation. Raw images at 530 nm and 625 nm were analyzed for changes in oxy- and deoxy- hemoglobin using the modified Beer-Lambert relationship as described previously (Sunil et al., 2020; Dunn et al., 2005).

4.6. GCaMP fluorescence correction for hemodynamic crosstalk

Calcium dynamics were analyzed as a change in fluorescence over time from the interspersed raw images excited at 470 nm. The fluorescence data were corrected for hemodynamic crosstalk as hemodynamic changes contaminate the fluorescence signal at both the excitation and emission wavelengths. The change in calcium concentration is approximately equal to the change in GCaMP fluorescence scaled by a time-varying hemoglobin absorption factor at both the GCaMP excitation and emission wavelengths. To account for this crosstalk, we implemented a correction algorithm, which makes use of the Beer-Lambert calculations, and which has been previously described by Ma et al (Ma, 2016). We have modified the previously described correction algorithm to account for changes in tissue optical properties in the stroke core.

The change in measured fluorescence intensity, accounting for crosstalk, is given by:

$$\frac{\Delta F(t)}{F_0} = e^{-\left(\Delta\mu_{a,ex}(t)x_{ex} + \Delta\mu_{a,em}(t)x_{em}\right)}.\frac{\Delta c_{GCaMP}(t)}{c_{0,GCaMP}(t)}$$

where F_0 and c_0 are the average of the trial over time, μ_a is the absorption coefficient over time at the excitation and emission wavelengths, and x is the pathlength of light traveled in the tissue at the excitation and emission wavelengths. Oxy- and deoxy-hemoglobin are the primary absorbing components in brain tissue and the absorption coefficient can be expressed as:

$$\Delta\mu_a(\lambda, t) = \epsilon_{HbO}(\lambda)\Delta HbO(t) + \epsilon_{HbR}(\lambda)\Delta HbR(t)$$

using the simultaneously obtained HbO and HbR measures and previously calculated molar extinction coefficients. The pathlength factor used for correction is obtained from Monte Carlo simulations of photon transport using the Monte Carlo eXtreme (MCX) platform (Fang and Boas, 2009; Chen et al., 2012). The absorption and scattering coefficients required for MCX simulations were obtained from spatial frequency domain imaging (described above). For pre-stroke imaging, a single absorption and scattering coefficient, yielding a single pathlength, was used for correction of all pixels. The correction method was validated using GFP fluorescence that was independent of neural activity. There is a decrease in GFP fluorescence during evoked responses due to hemoglobin absorption of fluorescence (Supplementary Fig. 2e). Once the correction is applied, there is no detectable change in GFP fluorescence (Supplementary Fig. 2f).

After stroke, the absorption and scattering coefficients used were determined on a semi pixel-by-pixel basis. This modified correction technique was introduced in order to account for changes in tissue optical properties after stroke (Sunil, 2021; Srinivasan et al., 2013). A

Monte Carlo simulation was run on any pixel that had a scattering coefficient that was 30 % larger than the mean scattering coefficient of the control animals, using the respective absorption and scattering coefficients of that pixel obtained from SFDI (Supplementary Figs. 2 and 3). This new pathlength was used for the correction of pixels within the stroke region that had increased scattering. The attenuation correction applied spatial maps and temporal traces are shown in Fig. 1c.

4.7. Analysis of evoked responses

Evoked responses were analyzed across the full hemisphere as well as within the forelimb region. Raw wide-field reflectance images were used to manually draw outlines of the exposed brain region and mask extraneous dental cement and headframe applied during the surgical procedure. This brain mask for the ipsilesional and contralesional hemisphere was used for all further analysis of neuroimaging measures. When calculating evoked responses across the full hemisphere, an average response was calculated, for both fluorescence and hemodynamics data, for each mouse by taking the mean response amplitude during the 5 s stimulation period for all pixels within each hemisphere regardless of response amplitudes. To define the forelimb region, a peak response was calculated as the 99th percentile of response magnitude within the 5 s stimulation period. A percentile was used instead of an absolute value for the peak response to minimize any noisy results due to large outliers in the responses. The forelimb region was then defined as all pixels that responded to within 0.75 of the peak response amplitude during the stimulation period. A forelimb mask was drawn around the largest boundary of connected pixels within this threshold. For analysis of overlap of evoked response in pre- and post-stroke between GCaMP and HbO, HbR, and HbT, individual forelimb masks were generated. For all other analyses of changes to forelimb function, the forelimb mask generated for pre-stroke GCaMP data was used.

4.8. Analysis of neurovascular coupling

To assess the relationship between neural activity and hemodynamics, neurovascular coupling was modeled using linear least-squares deconvolution (LSD) (Ma, 2016). The cortical hemodynamic response is known to be a linear convolution of the cortical neural activity and an impulse response function (IRF). The impulse response function, also called the hemodynamic response function, is the hemodynamic response to a neural stimulus. In a linear system, the convolution can be expressed as $y = X*h$, and can be represented as:

$$\begin{bmatrix} y_1 \\ y_2 \\ \vdots \\ y_t \end{bmatrix} = \begin{bmatrix} x_1 & 0 & 0 & \cdots & 0 \\ x_2 & x_1 & 0 & \cdots & 0 \\ \vdots & \vdots & \vdots & \ddots & \vdots \\ x_t & x_{t-1} & x_{t-2} & \cdots & x_n \end{bmatrix} \begin{bmatrix} h_1 \\ h_2 \\ \vdots \\ h_n \end{bmatrix}$$

where X is the input to the system, which is the corrected GCaMP fluorescence signal, and the length n used is 15 sec (from -5 sec to 10 sec), y is the output of the system, which is the hemodynamic signal, and h is the system's impulse function. A 15 sec kernel size was chosen to include 5 secs of future GCaMP signal and 10 sec of past GCaMP signal to quantify the hemodynamic response function. 10 s of past neural activity was sufficient to capture the hemodynamic response function and further increasing the kernel size beyond 10 s of past neural activity did not affect the hemodynamic response function characteristics. A second order polynomial fit was used to remove slow fluctuations in the signal during LSD. A direct solution to the linear system could result in an ill-conditioned matrix and therefore a regularization term is added, and the solution is obtained by minimizing the cost function and setting the derivative of the cost function to zero, as described previously, and is given by:

$$h = \left(X^T X + \lambda I\right)^{-1} X^T y$$

The regularization term λ was chosen to be 0.1 through all the analysis. The deconvolution was performed on a pixel-by-pixel basis at each time point post-stroke. Global fluctuations in the GCaMP and hemodynamic time courses were regressed from the signals prior to model fitting.

4.9. Analysis of resting state functional connectivity

Global network connectivity changes following stroke were assessed using resting state functional connectivity as described previously by a number of groups (Wright et al., 2017; Chung, 2021; Xie, 2020). Time traces of HbO and GCaMP were bandpass filtered into two frequency bands, the typically used infraslow (0.008–0.09 Hz) frequency band and a higher frequency band (0.09–0.4 Hz) and regressed to remove any global fluctuations in the signal. To evaluate the strength of network connections to the affected forelimb region, a seed was placed in the center of the original forelimb somatosensory region of the affected hemisphere. The seed time trace was calculated by averaging the time trace within 0.25 mm of the seed location and connectivity was assessed by calculating the correlation between the seed time trace and the time course of every other pixel. By averaging the positive correlation coefficients between the forelimb seed and all pixels that lie in the contralesional forelimb region we calculated a forelimb connectivity map (Xie, 2020). Interhemispheric connectivity maps were calculated by correlating each pixel within the affected hemisphere with its mirror pixel, mirrored along the midline, in the unaffected hemisphere. The interhemispheric connectivity index was then calculated by averaging all the pixels within the homotopic map of the affected hemisphere (Xie, 2020). To assess the overall connectivity of the brain, global connectivity maps were generated by calculating the correlation of each pixel with every other pixel and then assigning the average positive correlation coefficient to that pixel. From the global connectivity maps, a global connectivity index was calculated by taking the mean of the correlation coefficients for all pixels within the map (Xie, 2020).

4.10. Targeted photothrombosis

Focal cerebral ischemia was performed using an optimized photothrombosis method described previously (Sunil et al., 2020). A distal branch of the middle cerebral artery supplying the forelimb somatosensory region, determined through pre-stroke forelimb stimulation, was targeted for occlusion. A 520 nm laser diode with axial and lateral parameters of 104 μm and 6 μm was tuned to a minimal post-objective power of 0.6 mW. These parameters were designed to occlude only the target vessel and prevent laser damage to the surrounding tissue, thus ensuring that the ischemia procedure was physiological in nature. Real-time changes to cerebral blood flow (CBF) were monitored through laser speckle contrast imaging (LSCI). Ten minutes of baseline CBF was obtained following which the mouse was lightly anesthetized to inject Rose Bengal (100 μl, 15 mg/ml in saline) retroorbitally. The mouse was then immediately taken off isoflurane and allowed to recover, which was determined by a return of CBF to baseline and the mouse exhibiting natural behaviors such as whisking. Following recovery, the green laser was turned on until the target vessel was occluded, as indicated by the target branch disappearing on LSCI. Once the target branch was occluded, the laser power was reduced to 0.5 mW for an additional minute and then turned off. If at any point the target branch started flowing again, the laser was turned back on until occlusion. Additionally, as described previously, two collateral branches were also targeted to obtain a stable infarct. The procedure was followed for 1 h from the initiation of photothrombosis.

4.11. Infarct assessment

SFDI was used to obtain the spatial extent of the stroke core, which was then used to produce peri-infarct and healthy tissue boundaries. To determine the stroke area, which we define as the stroke core, a built in Matlab function activecontour, was used. Activecontour is an iterative region-growing technique that builds a boundary within an image based on user defined initial curves. A user defined curve was drawn within the stroke region and the algorithm evolved a curve to the object boundary. This final contour was used as the stroke core (Sunil, 2021). Supplementary figure 1 shows the stroke core outline for 6 mice (left) and the distribution of infarct size for all mice (right). The peri-infarct zone was defined as the region that extended 0.5 mm outward from the stroke core outline. The Matlab function imdilate was used to expand the core contour uniformly from the boundary by 0.5 mm. Brain tissue beyond the core outline and within the expanded boundary was considered the peri-infarct and tissue outside the expanded boundary was considered healthy. This process was repeated at each time point. The outlines produced at Week1 were used as reference outlines in pre-stroke healthy conditions.

4.12. Behavioral testing

The cylinder test was used in all mice to assess behavioral deficit in forelimb use over the course of 4 weeks following stroke. Two sessions of pre-stroke testing was obtained the week before stroke induction to assess basal preference in forepaw use. Following photothrombotic stroke, mice were tested at 2 days, 1 week, 2 weeks, and 4 weeks. Each testing session involved placing a mouse in a clear glass cylinder and videotaping its natural behavior from below for 15 min. Forelimb use was assessed by counting the number of times the mouse used each forelimb to make first contact with the cylinder wall during rears. Asymmetry in forelimb use after stroke was quantified as a percent change from baseline use of the contralateral (affected) forelimb. Change from baseline was used to compensate for the fact that some mice prefer one paw over the other even before a stroke. Raw forelimb rears for each mouse is reported in Supplementary table 1.

4.13. Data analysis and statistics

All data was analyzed offline using custom Matlab codes. Image analysis for SFDI, calcium fluorescence, and evoked and resting-state intrinsic optical signal imaging has been outlined in previous sections. The dice similarity coefficient for area overlap in evoked responses and RSFC is calculated using the Matlab function dice.m. The dice coefficient is twice the ratio of the intersection of two binary images and the sum of the number of elements in each image, given by:

$$dice(A, B) = \frac{2|A \cap B|}{|A| + |B|}$$

Goodness-of-fit correlation and significance for stimulus evoked response magnitudes of GCaMP and hemodynamics were made using a linear fit. All statistical analyses were made using Matlab with *post hoc* comparisons using t-tests. A two sample students *t*-test was performed for comparing data points with pre-stroke data (Matlab function: ttest2).

CRediT authorship contribution statement

Smrithi Sunil: Conceptualization, Methodology, Investigation, Visualization, Visualization. **John Jiang:** Methodology. **Shashwat Shah:** Investigation, Visualization. **Sreekanth Kura:** Methodology. **Kivilcim Kilic:** Conceptualization, Methodology. **Sefik Evren Erdener:** Conceptualization, Methodology. **Cenk Ayata:** Supervision. **Anna Devor:** Supervision. **David A. Boas:** Conceptualization, Methodology, Visualization, Supervision.

Declaration of Competing Interest

The authors declare that they have no known competing financial interests or personal relationships that could have appeared to influence the work reported in this paper.

Data availability

Analysis scripts, link to corresponding datasets, and data descriptions are available on the Boston University Neurophotonics Center Github. Link to github repository: https://github.com/BUNPC/NeurovascularCouplingStroke.

Acknowledgment

Appendix A. Supplementary data

Supplementary data to this article can be found online at https://doi.org/10.1016/j.nicl.2023.103377.

References

Adaikkan, C. *et al.* Gamma Entrainment Binds Higher-Order Brain Regions and Offers Neuroprotection. *Neuron* 102, 929-943.e8 (2019).

Angels Font, M., Arboix, A., Krupinski, J.A., 2010. Neurogenesis and Neuroplasticity in Ischemic Stroke. Curr. Cardiol. Rev. 6, 238–244.

Attwell, D., Buchan, A.M., Charpak, S., Lauritzen, M., MacVicar, B.A., Newman, E.A., 2010. Glial and neuronal control of brain blood flow. Nature 468 (7321), 232–243.

Balbi, M., et al., 2021. Gamma frequency activation of inhibitory neurons in the acute phase after stroke attenuates vascular and behavioral dysfunction. Cell Rep. 34, 108696.

Bauer, A.Q., Kraft, A.W., Wright, P.W., Snyder, A.Z., Lee, J.-M., Culver, J.P., 2014. Optical imaging of disrupted functional connectivity following ischemic stroke in mice. Neuroimage 99, 388–401.

Blaschke, S.J., Hensel, L., Minassian, A., Vlachakis, S., Tscherpel, C., Vay, S.U., Rabenstein, M., Schroeter, M., Fink, G.R., Hoehn, M., Grefkes, C., Rueger, M.A., 2021. Translating Functional Connectivity after Stroke: Functional Magnetic Resonance Imaging Detects Comparable Network Changes in Mice and Humans. Stroke 52 (9), 2948–2960.

Boyd, L.A., Hayward, K.S., Ward, N.S., Stinear, C.M., Rosso, C., Fisher, R.J., Carter, A.R., Leff, A.P., Copland, D.A., Carey, L.M., Cohen, L.G., Basso, D.M., Maguire, J.M., Cramer, S.C., 2017. Biomarkers of stroke recovery: Consensus-based core recommendations from the Stroke Recovery and Rehabilitation Roundtable. Int. J. Stroke 12 (5), 480–493.

Brown, C.E., Aminoltejari, K., Erb, H., Winship, I.R., Murphy, T.H., 2009. In Vivo Voltage-Sensitive Dye Imaging in Adult Mice Reveals That Somatosensory Maps Lost to Stroke Are Replaced over Weeks by New Structural and Functional Circuits with Prolonged Modes of Activation within Both the Peri-Infarct Zone and Distant Sites. J. Neurosci. 29, 1719–1734.

Bütefisch, C.M., Netz, J., Weßling, M., Seitz, R.J., Hömberg, V., 2003. Remote changes in cortical excitability after stroke. Brain 126, 470–481.

Buxton, R.B., Griffeth, V.E.M., Simon, A.B., Moradi, F., 2014. Variability of the coupling of blood flow and oxygen metabolism responses in the brain: A problem for interpreting BOLD studies but potentially a new window on the underlying neural activity. Front. Neurosci. 8, 1–6.

Carmichael, S.T., 2005. Rodent models of focal stroke: Size, mechanism, and purpose. NeuroRX 2 (3), 396–409.

Carmichael, S.T., 2012. Brain excitability in stroke: The yin and yang of stroke progression. Arch. Neurol. 69, 161–167.

Carmichael, S.T., Chesselet, M.F., 2002. Synchronous neuronal activity is a signal for axonal sprouting after cortical lesions in the adult. J. Neurosci. 22, 6062–6070.

Carter, A.R., Astafiev, S.V., Lang, C.E., Connor, L.T., Rengachary, J., Strube, M.J., Pope, D.L.W., Shulman, G.L., Corbetta, M., 2009. Resting state inter-hemispheric fMRI connectivity predicts performance after stroke. Ann. Neurol. NA–NA.

Cassidy, J.M., Cramer, S.C., 2017. Spontaneous & Therapeutic-Induced Mechanisms of Functional Recovery After Stroke. Transl. Stroke Res. 8, 33–46.

Chen, J., Fang, Q., Intes, X., 2012. Mesh-based Monte Carlo method in time-domain widefield fluorescence molecular tomography. J. Biomed. Opt. 17, 1.

Chen, T.-W., Wardill, T.J., Sun, Y.i., Pulver, S.R., Renninger, S.L., Baohan, A., Schreiter, E.R., Kerr, R.A., Orger, M.B., Jayaraman, V., Looger, L.L., Svoboda, K., Kim, D.S., 2013. Ultrasensitive fluorescent proteins for imaging neuronal activity. Nature 499 (7458), 295–300.

Chung, D.Y., et al., 2021. Subarachnoid hemorrhage leads to early and persistent functional connectivity and behavioral changes in mice. J. Cereb. Blood Flow Metab. 41, 975–985.

Clarkson, A.N., et al., 2013. Multimodal examination of structural and functional remapping in the mouse photothrombotic stroke model. J. Cereb. Blood Flow Metab. 33, 716–723.

Corbetta, M., 2012. Functional connectivity and neurological recovery. Dev. Psychobiol. 54, 239–253.

Cramer, S.C., 2008. Repairing the human brain after stroke: I. Mechanisms of spontaneous recovery. *Ann. Neurol.* 63, 272–287.

Cramer, J.V., Gesierich, B., Roth, S., Dichgans, M., Düring, M., Liesz, A., 2019. In vivo widefield calcium imaging of the mouse cortex for analysis of network connectivity in health and brain disease. Neuroimage 199, 570–584.

Cuccia, D.J., Bevilacqua, F., Durkin, A.J., Ayers, F.R., Tromberg, B.J., 2009. Quantitation and mapping of tissue optical properties using modulated imaging. J. Biomed. Opt. 14, 024012.

Culver, J.P., Siegel, A.M., Franceschini, M.A., Mandeville, J.B., Boas, D.A., 2005. Evidence that cerebral blood volume can provide brain activation maps with better spatial resolution than deoxygenated hemoglobin. Neuroimage 27 (4), 947–959.

Dana, H., Chen, T.-W., Hu, A., Shields, B.C., Guo, C., Looger, L.L., Kim, D.S., Svoboda, K., Arenkiel, B., 2014. Thy1-GCaMP6 transgenic mice for neuronal population imaging in vivo. PLoS One 9 (9), e108697.

Dunn, A.K., Devor, A., Dale, A.M., Boas, D.A., 2005. Spatial extent of oxygen metabolism and hemodynamic changes during functional activation of the rat somatosensory cortex. Neuroimage 27 (2), 279–290.

Erinjeri, J.P., Woolsey, T.A., 2002. Spatial integration of vascular changes with neural activity in mouse cortex. J. Cereb. Blood Flow Metab. 22, 353–360.

Fang, Q., Boas, D.A., 2009. Monte Carlo Simulation of Photon Migration in 3D Turbid Media Accelerated by Graphics Processing Units. Opt. Express 17 (22), 20178.

Girouard, H., Iadecola, C., 2012. Neurovascular coupling in the normal brain and in hypertension, stroke, and Alzheimer disease Regulation of the Cerebral Circulation stroke. and Alzheimer disease. 10021, 328–335.

Goltsov, A., et al., 2017. Bifurcation in blood oscillatory rhythms for patients with ischemic stroke: A small scale clinical trial using laser Doppler flowmetry and computational modeling of vasomotion. Front. Physiol. 8, 1–11.

Grefkes, C., Fink, G.R., 2011. Reorganization of cerebral networks after stroke: New insights from neuroimaging with connectivity approaches. Brain 134 (5), 1264–1276.

Grefkes, C., Fink, G.R., 2014. Connectivity-based approaches in stroke and recovery of function. Lancet Neurol. 13, 206–216.

Hamel, E., 2006. Perivascular nerves and the regulation of cerebrovascular tone. J. Appl. Physiol. 100 (3), 1059–1064.

Harrison, T.C., Silasi, G., Boyd, J.D., Murphy, T.H., 2013. Displacement of sensory maps and disorganization of motor cortex after targeted stroke in mice. Stroke 44 (8), 2300–2306.

He, F., et al., 2020. Multimodal mapping of neural activity and cerebral blood flow reveals long-lasting neurovascular dissociations after small-scale strokes. Sci. Adv. 6, 1–13.

Huang, M. X. *et al.* Marked Increases in Resting-State MEG Gamma-Band Activity in Combat-Related Mild Traumatic Brain Injury. *Cereb. Cortex* 30, 283–295 (2020).

Intaglietta, M., 1990. Vasomotion and flowmotion: physiological mechanisms and clinical evidence. Vasc. Med. Rev. vmr-1 (2), 101–112.

Intaglietta, M. Arteriolar Vasomotion: Implications for Tissue Ischemia. *J. Vasc. Res.* 28 (suppl 1, 1–7 (1991).

Isaacson, J., Scanziani, M., 2011. How inhibition shapes cortical activity. Neuron 72 (2), 231–243.

Johansen-Berg, H. *et al.* Correlation between motor improvements and altered fMRI activity after rehabilitative therapy. *Brain* 125, 2731–2742 (2002).

Jones, T.A., 2017. Motor compensation and its effects on neural reorganization after stroke. Nat. Rev. Neurosci. 18 (5), 267–280.

Joy, M.T., Carmichael, S.T., 2021. Encouraging an excitable brain state: mechanisms of brain repair in stroke. Nat. Rev. Neurosci. 22, 38–53.

Kim, T.H., et al., 2016. Long-Term Optical Access to an Estimated One Million Neurons in the Live Mouse Cortex. Cell Rep. 17, 3385–3394.

Kleinfeld, D., et al., 2011. A guide to delineate the logic of neurovascular signaling in the brain. Front. Neuroenergetics 3, 1–9.

Kunz, A., Iadecola, C., 2009. Cerebral vascular dysregulation in the ischemic brain. Handb. Clin. Neurol. 92, 283–305.

Kura, S., Xie, H., Fu, B., Ayata, C., Boas, D.A., Sakadžić, S., 2018. Intrinsic optical signal imaging of the blood volume changes is sufficient for mapping the resting state functional connectivity in the rodent cortex. J. Neural Eng. c 15 (3), 035003.

Laaksonen, K., Helle, L., Parkkonen, L., Kirveskari, E., Mäkelä, J.P., Mustanoja, S., Tatlisumak, T., Kaste, M., Forss, N., Chacron, M.J., 2013. Alterations in Spontaneous Brain Oscillations during Stroke Recovery. PLoS One 8 (4), e61146.

Lake, E.M.R., et al., 2020. Simultaneous cortex-wide fluorescence Ca2+ imaging and whole-brain fMRI. Nat. Methods 17, 1262–1271.

Lake, E.M.R., Bazzigaluppi, P., Stefanovic, B., 2016. Functional magnetic resonance imaging in chronic ischaemic stroke. Philos. Trans. R. Soc. B Biol. Sci. 371, 1–11.

Lim, D.H., LeDue, J.M., Mohajerani, M.H., Murphy, T.H., 2014. Optogenetic Mapping after Stroke Reveals Network-Wide Scaling of Functional Connections and Heterogeneous Recovery of the Peri-Infarct. J. Neurosci. 34, 16455–16466.

Lo, E.H., Dalkara, T., Moskowitz, M.A., 2003. Neurological diseases: Mechanisms, challenges and opportunities in stroke. Nat. Rev. Neurosci. 4, 399–414.

Lo, E.H., Moskowitz, M.A., Jacobs, T.P., 2005. Exciting, radical, suicidal: How brain cells die after stroke. Stroke 36 (2), 189–192.

Logothetis, N.K., Pauls, J., Augath, M., Trinath, T., Oeltermann, A., 2001. Neurophysiological investigation of the basis of the fMRI signal. Nature 412 (6843), 150–157.

Luo, L., Callaway, E.M., Svoboda, K., 2018. Genetic Dissection of Neural Circuits: A Decade of Progress. Neuron 98 (2), 256–281.

Ma, Y., et al., 2016. High-speed, wide-field optical mapping (WFOM) of neural activity and brain haemodynamics: Considerations and novel approaches. Under Rev. 371, 20150360.

Ma, Y. *et al.* Resting-state hemodynamics are spatiotemporally coupled to synchronized and symmetric neural activity in excitatory neurons. *Proc. Natl. Acad. Sci.* 113, E8463–E8471 (2016).

Mateo, C., Knutsen, P.M., Tsai, P.S., Shih, A.Y., Kleinfeld, D., 2017. Entrainment of Arteriole Vasomotor Fluctuations by Neural Activity Is a Basis of Blood-Oxygenation-Level-Dependent "Resting-State" Connectivity. Neuron 96 (4), 936–948.e3.

modeling cerebral ischemia, 2010. Bacigaluppi, M., Comi, G. & Hermann, D. M. Animal models of ischemic stroke. Part two. Open Neurol. J. 4, 34–38.

Mohajerani, M. H., Aminoltejari, K. & Murphy, T. H. Targeted mini-strokes produce changes in interhemispheric sensory signal processing that are indicative of disinhibition within minutes. *Proc. Natl. Acad. Sci.* 108, E183–E191 (2011).

Montgomery, M.K., et al., 2020. Glioma-Induced Alterations in Neuronal Activity and Neurovascular Coupling during Disease Progression. Cell Rep. 31, 107500.

Moseley, M., 2010. Mri of stroke. Imaging 41, 410–414.

Moskowitz, M.A., Lo, E.H., Iadecola, C., 2010. The science of stroke: Mechanisms in search of treatments. Neuron 67 (2), 181–198.

Park, C.-H., Chang, W.H., Ohn, S.H., Kim, S.T., Bang, O.Y., Pascual-Leone, A., Kim, Y.-H., 2011. Longitudinal changes of resting-state functional connectivity during motor recovery after stroke. Stroke 42 (5), 1357–1362.

Pineiro, R., Pendlebury, S., Johansen-Berg, H., Matthews, P.M., 2002. Altered hemodynamic responses in patients after subcortical stroke measured by functional MRI. Stroke 33 (1), 103–109.

Rabiller, G., He, J.W., Nishijima, Y., Wong, A., Liu, J., 2015. Perturbation of brain oscillations after ischemic stroke: A potential biomarker for post-stroke function and therapy. Int. J. Mol. Sci. 16, 25605–25640.

Rehme, A.K., Eickhoff, S.B., Wang, L.E., Fink, G.R., Grefkes, C., 2011. Dynamic causal modeling of cortical activity from the acute to the chronic stage after stroke. Neuroimage 55 (3), 1147–1158.

Rehme, A.K., Eickhoff, S.B., Rottschy, C., Fink, G.R., Grefkes, C., 2012. Activation likelihood estimation meta-analysis of motor-related neural activity after stroke. Neuroimage 59 (3), 2771–2782.

Schrandt, C.J., Kazmi, S.S., Jones, T.A., Dunn, A.K., 2015. Chronic Monitoring of Vascular Progression after Ischemic Stroke Using Multiexposure Speckle Imaging and Two-Photon Fluorescence Microscopy. J. Cereb. Blood Flow Metab. 35, 933–942.

Sharma, N., Cohen, L.G., 2012. Recovery of motor function after stroke. Dev. Psychobiol. 54, 254–262.

Shih, Y.Y.I., et al., 2014. Imaging neurovascular function and functional recovery after stroke in the rat striatum using forepaw stimulation. J. Cereb. Blood Flow Metab. 34, 1483–1492.

Sommer, C.J., 2017. Ischemic stroke: experimental models and reality. Acta Neuropathol. 133 (2), 245–261.

Srinivasan, V.J., Mandeville, E.T., Can, A., Blasi, F., Climov, M., Daneshmand, A., Lee, J. H., Yu, E., Radhakrishnan, H., Lo, E.H., Sakadžić, S., Eikermann-Haerter, K., Ayata, C., Georgakoudi, I., 2013. Multiparametric, Longitudinal Optical Coherence Tomography Imaging Reveals Acute Injury and Chronic Recovery in Experimental Ischemic Stroke. PLoS One 8 (8), e71478.

Stinear, C.M., 2017. Prediction of motor recovery after stroke: advances in biomarkers. Lancet Neurol. 16 (10), 826–836.

Sunil, S., et al., 2021. NeuroImage : Clinical Stroke core revealed by tissue scattering using spatial frequency domain imaging. NeuroImage Clin. 29, 102539.

Sunil, S., Erdener, S.E., Lee, B.S., Postnov, D., Tang, J., Kura, S., Cheng, X., Chen, I.A., Boas, D.A., Kilic, K., 2020. Awake chronic mouse model of targeted pial vessel occlusion via photothrombosis. Neurophotonics 7 (01), 1.

Tian, L., et al., 2009. Imaging neural activity in worms, flies and mice with improved GCaMP calcium indicators. Nat. Methods 6, 875–881.

Valley, M.T., et al., 2020. Separation of hemodynamic signals from GCaMP fluorescence measured with wide-field imaging. J. Neurophysiol. 123, 356–366.

van Meer, M.P.A., et al., 2010. Recovery of Sensorimotor Function after Experimental Stroke Correlates with Restoration of Resting-State Interhemispheric Functional Connectivity. J. Neurosci. 30, 3964–3972.

Veldsman, M., Cumming, T., Brodtmann, A., 2015. Beyond BOLD: Optimizing functional imaging in stroke populations. Hum. Brain Mapp. 36, 1620–1636.

Weber, R., et al., 2008. Early prediction of functional recovery after experimental stroke: Functional magnetic resonance imaging, electrophysiology, and behavioral testing in rats. J. Neurosci. 28, 1022–1029.

White, B.R., Bauer, A.Q., Snyder, A.Z., Schlaggar, B.L., Lee, J.-M., Culver, J.P., Sporns, O., 2011. Imaging of functional connectivity in the mouse brain. PLoS One 6 (1), e16322.

Winder, A.T., Echagarruga, C., Zhang, Q., Drew, P.J., 2017. Weak correlations between hemodynamic signals and ongoing neural activity during the resting state. Nat. Neurosci. 20, 1761–1769.

Winship, I.R., Murphy, T.H., 2008. In Vivo Calcium Imaging Reveals Functional Rewiring of Single Somatosensory Neurons after Stroke. J. Neurosci. 28, 6592–6606.

Wright, P.W., Brier, L.M., Bauer, A.Q., Baxter, G.A., Kraft, A.W., Reisman, M.D., Bice, A. R., Snyder, A.Z., Lee, J.-M., Culver, J.P., Marinazzo, D., 2017. Functional connectivity structure of cortical calcium dynamics in anesthetized and awake mice. PLoS One 12 (10), e0185759.

Xie, H., et al., 2020. Differential effects of anesthetics on resting state functional connectivity in the mouse. J. Cereb. Blood Flow Metab. 40, 875–884.

Xu, Y., Zou, P., Cohen, A.E., 2017. Voltage imaging with genetically encoded indicators. Curr. Opin. Chem. Biol. 39, 1–10.